RSC Advances

REVIEW

View Article Online
View Journal | View Issue

Cite this: *RSC Adv.*, 2023, **13**, 10958

Visible-light acridinium-based organophotoredox catalysis in late-stage synthetic applications

Praveen P. Singh, [a] Jaya Singh[b] and Vishal Srivastava *[c]

Received 28th February 2023
Accepted 29th March 2023

DOI: 10.1039/d3ra01364b

rsc.li/rsc-advances

The field of photoredox catalysis has been transformed by the use of organic photocatalysts, which give access to re-activities that were previously only possible with transition-metal photocatalysts. Recent advancements in the use of an acridinium photocatalyst in organic synthesis are covered in this review. Both the late-stage functionalization of biorelevant molecules and the activation of inert chemical bonds are explored, with an emphasis on their mechanistic features.

1. Introduction

Photoredox catalysis has quickly become a platform for the development of synthetic techniques over the past decade as it exhibits a pioneering approach for molecular functionalization[1–3] and has made a significant impact on organic chemistry. The importance of light to form chemical bonds under benign conditions has grown significantly, and visible-light photoredox catalysis has attracted huge attention.[4–11] A century ago, the visionary scientist Giacomo Ciamcian emphasised the need to develop technology that allowed the conversion of light into chemicals and fuels[12] after recognizing the impact of light to initiate redox transformations that use low-energy visible light and, through photoinduced electron transfer (PET), produces highly reactive intermediates under mild operating conditions. This has enabled to the development of a wide range of reactions, including the synthesis of complex compounds.[13] Iridium and ruthenium-based photocatalysts are frequently used in many of those photoreactions due to the high redox potentials and the comparatively prolonged lives of their excited states. In fact, the photophysical and electrochemical properties of the photocatalysts can potentially be changed by a modest modification of the ligand structure. Even though, the commercially available organic dyes like eosin Y[14] and flavins[15–17] have demonstrated interesting photochemical properties as photocatalysts, variation of their molecular scaffolds is frequently complicated, which inhibits the use of structurally related photocatalysts with different photochemical properties. Recent efforts have concentrated on devising practically simple and modular syntheses to access new and effective organophotocatalysts[18,19] in order to close this gap and create entirely organic, less

[a]*Department of Chemistry, United College of Engineering & Research, Naini, Prayagraj, 211010, India. E-mail: ppsingh23@gmail.com*
[b]*Department of Chemistry, LRPG College, Sahibabad, Gaziabad, Uttar Pradesh, India*
[c]*Department of Chemistry, CMP Degree College, University of Allahabad, Prayagraj, 211002, Uttar Pradesh, India. E-mail: vishalgreenchem@gmail.com*

Praveen P. Singh is working as Assistant Professor in the Department of Chemistry at the United College of Engineering and Research, Prayagraj, India. He obtained his BSc, MSc in Organic Chemistry from T. D. P. G. College (V. B. S Purvanchal University) Jaunpur and DPhil. from Department of Chemistry, University of Allahabad, India. His current research interests include the development of synthetic receptors for the recognition of biological target structures and the application of visible light chemical photo-catalysis towards organic synthesis as well as nanophotocatalysis.

Jaya Singh is an Assistant Professor in the Department of Chemistry, LRPG College, Sahibabad, Ghaziabad, Uttar Pradesh, India. She has done her graduation and post-graduation from the University of Allahabad. She also obtained her DPhil. Degree from the University of Allahabad, India. She was the topper in BSc and gold medalist in MSc (Chemistry). She has over 17 years of teaching and research experience in varied fields. Her field of research is synthetic organic chemistry and green chemistry.

expensive, long-lasting, and environmentally benign photocatalysts.

In this context, ruthenium and iridium catalysts serve as particularly adaptable scaffolds in the field of photoredox catalysis, which has been transformed by polypyridyl transition metal complexes. They are incredibly valuable catalysts for photochemical transformations because of the broad range of characteristics resulting from the tunability of their ligands. With the invention of entirely organic substitutes, opportunities for potentially sustainable approaches emerged. Acridinium salts, developed by Fukuzumi[20,21] are one of them and are known to exhibit exceptional photophysical properties that complement those of polypyridyl transition metal complexes. They are excellent photocatalysts for a plethora of preparative transformations owing to their strong reduction potential in the excited state, stability, pH independence, and dissolution rate in a wide range of solvents.

As depicted in (Scheme 1),[22–25] upon irradiation, an excited photocatalyst (PC*) can act as an electron shuttle, interacting with sacrificial electron donor D (path I) or acceptors A (path II) to yield either a strongly reducing or oxidizing catalyst toward organic substrates S. PC* can also directly transfer energy to an organic substrate to yield electronically excited species (path III). Depending on the reaction conditions, the inverse events can occur to complete a reductive quenching cycle. Moreover, a PC can also transfer its excited state energy to a substrate or reagent that is not able to absorb light at the given wavelength, thereby inducing a chemical reaction. The combination of photocatalysis with transition metal catalysis generates metallaphotocatalysis,[26,27] that enables selective carbon-heteroatom and carbon–carbon cross-coupling reactions under benign conditions. It also significantly affects the synthesis of small molecules and also plays a crucial role in late stage functionalization of organic molecules.

Furthermore, recent synthetic studies have demonstrated that due to the distinctive modularity of acridinium salts, the structural changes made by using these catalyst preparation techniques[28] can significantly alter the photophysical and electrochemical properties.[29] In continuation of our work on photocatalysed organic synthesis[30,31] this review aims to provide a comprehensive report on the current research, especially the role of acridinium salts in the organic synthesis and late stage chemical transformations.

Vishal Srivastava is working as Assistant Professor, Department of Chemistry, C. M. P. College, (Constituent P. G. College of Central University of Allahabad) Prayagraj, India. He has completed BSc, MSc in Organic Chemistry and Doctoral Degree (DPhil.) from Department of Chemistry, University of Allahabad, India. His current research work involves the designing of novel biologically active photoredox catalysed synthesis of organic compounds.

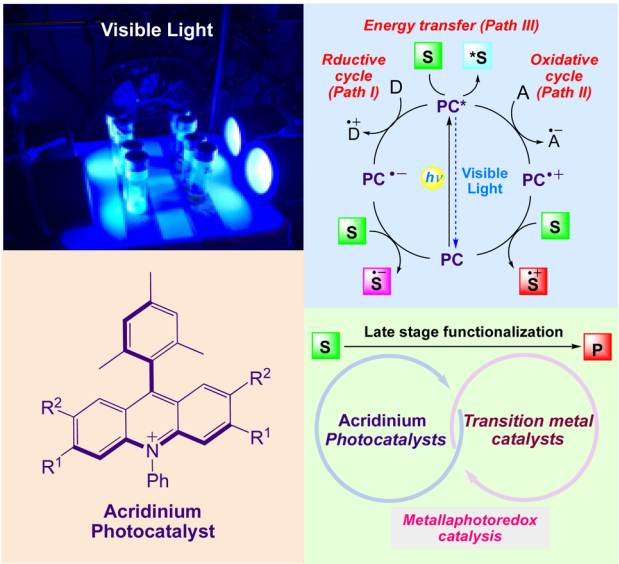

Scheme 1 General mechanism of visible light induced acridinium photocatalyst for synthesis of organic compounds.

2. Synthesis of acridinium-based photocatalyst

The polypyridyl complexes of ruthenium and iridium are now the leading catalysts for PET-based catalysis because of their substantial excited-state lifetimes and adaptable redox potentials.[32–34]

Despite their usefulness, their sustainability is a matter of concern due to their high cost and dependency on precious metals. Organic dyes offer an intriguing substitute, such as the acridinium salt that Fukuzumi (**1′**, Scheme 2A)[35,36] initially introduced and Nicewicz (Scheme 2B)[37] popularised as a photoredox catalyst. The stability and photophysical characteristics of acridinium-based photoredox catalysis have improved as a result of structural changes made to the catalyst's core. By adding 1,5-bifunctional nucleophiles to aromatic esters, Sparr and co-workers demonstrated an effective method for producing acridinium salts that are rich in electrons (Scheme 2C).[38,39] Mancheño and co-workers developed a synthetic strategy based on a novel straightforward oxidative Ugi-type reaction at the benzylic position of C9-unsubstituted acridanes (Scheme 2D).[35a] Nicewicz also created a library of unique acridinium salts using this adaptable method and evaluated their photophysical characteristics (Scheme 2E).[35b]

3. Late-stage acridinium diversification

Sparr[40] in 2021 described an ad-hoc approach for preparing acridinium salts with a particularly wide range of photoredox characteristics. The process involves connecting an aryne–

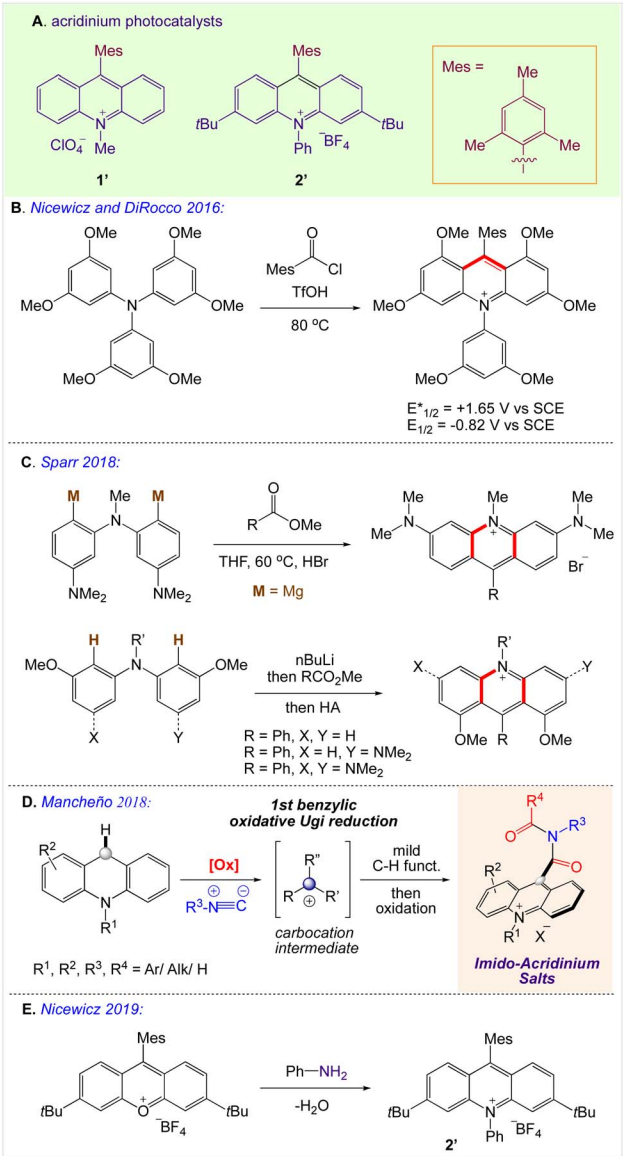

Scheme 2 Synthesis of acridinium-based photoredox catalysts.

imine aryne to a key component of tetrafluoro acridinium salt for nucleophilic aromatic substitution reactions that result in the formation of diaminoacridinium and unidentified azarhodol photo-catalysts during the late stages of diversification. The organic acridinium photocatalysts are suitable for bifunctional photoredox catalysis and organocatalytic photochemical C–N cross-couplings due to their diverse functionalities and redox characteristics (Scheme 3).

A highly functional group-tolerant (*e.g.*, halogen, nitrile, ketone, ester, and nitro) photoinduced arylation of *N*-substituted acridinium salts has been devised by Soule and co-workers[41] in 2022. A wide variety of C9-arylated acridinium-based catalysts with precisely calibrated excited-state lifetimes and redox potentials have been generated in a single process. Later on, the photoredox-catalyzed fragmentation of 1,2-diol derivatives using these functionalized acridinium salts was assessed (lignin models). For the selective $C^{\beta}O$–Ar bond

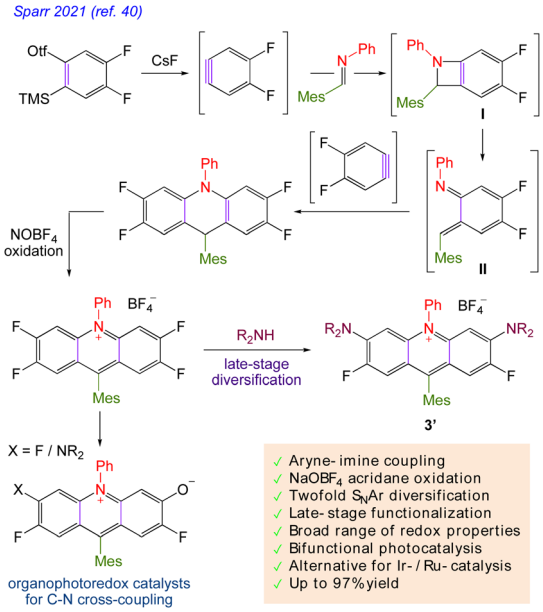

Scheme 3 Late-stage acridinium diversification.

breakage of diol monoarylethers to produce 1,2-diols in good yields, 2-bromophenyl substituted *N*-methyl acridinium has excelled all photoredox catalysts, including commercial Fukuzumi's catalyst.

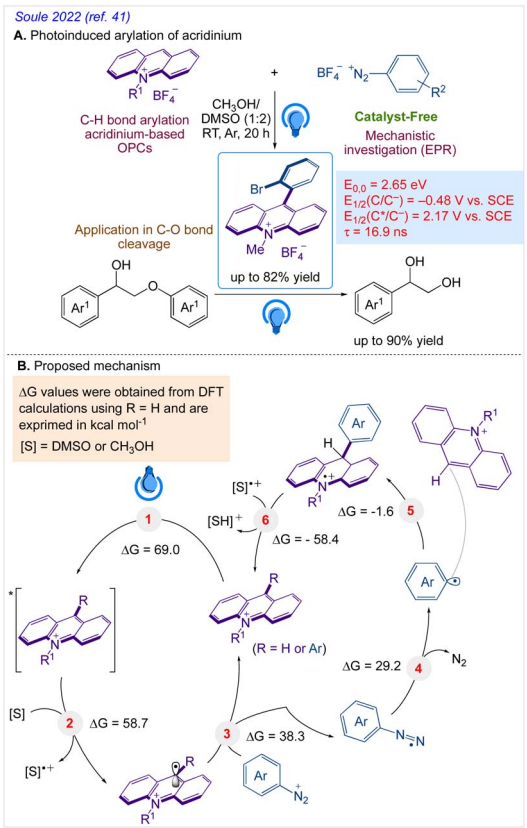

Scheme 4 (A) Late-stage photoinduced arylation of acridinium salts. (B) Proposed mechanism for the photoinduced C9 arylation of *N*-methyl acridinium salts with aryl diazonium salts.

Table 1 Photophysical properties of the acridinium based photocatalyst

Entry	Acridinium based photocatalyst	$E_{0,0}$[a] [eV]	$E_{1/2}$ (C/C^{-})[b] [V *vs.* SCE]	$E_{1/2}$ (C^{*}/C^{-})[c] [V *vs.* SCE]	λ_{abs}[d] [nm] ($\varepsilon \times 10^{3}$ [M^{-1} cm^{-1}])	λ_{em}[e] [nm]	τ[f] [ns]	Ref.
1	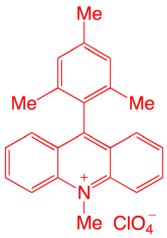 Fukuzumi catalyst	2.57	−0.57	2.08	425	—	6	29
2	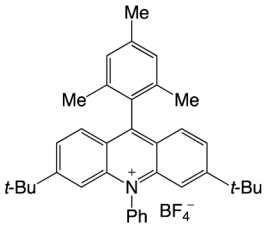	2.66	−0.59	2.08	420	517	14.4	29
3	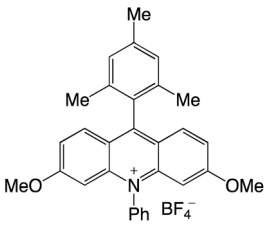	—	−0.71	2.01	407	525	3.0	29
4	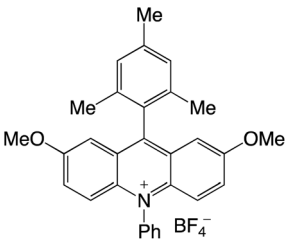	—	−0.57	1.90	466	545	18.7	29
5	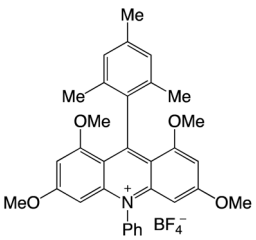	—	−0.84	1.62	412	550	1.3, 8.9	29
6	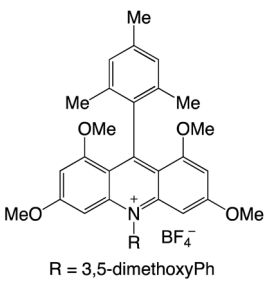 R = 3,5-dimethoxyPh	—	−0.82	1.65	414	550	1.3, 12.3	29

Table 1 (*Contd.*)

Entry	Acridinium based photocatalyst	$E_{0,0}$[a] [eV]	$E_{1/2}$ (C/C^{-})[b] [V *vs.* SCE]	$E_{1/2}$ (C^{*}/C^{-})[c] [V *vs.* SCE]	λ_{abs}[d] [nm] ($\varepsilon \times 10^{3}$ [M^{-1} cm^{-1}])	λ_{em}[e] [nm]	τ[f] [ns]	Ref.
7	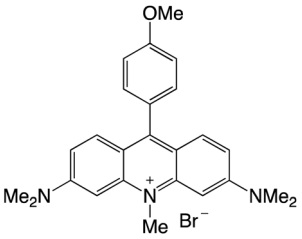	2.41	−1.15	1.26	501	531	—	29
8	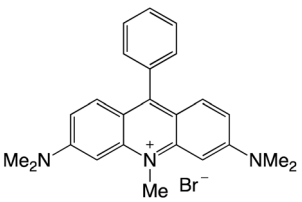	2.40	−1.10	1.30	502	534	—	29
9	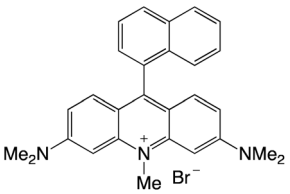	2.39	−1.13	1.26	506	534	—	29
10	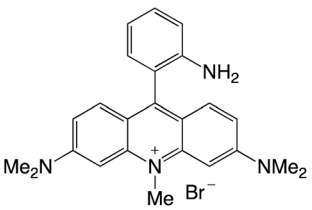	2.39	−1.14	1.25	506	532	—	29
11	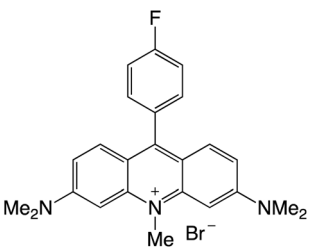	2.40	−1.12	1.28	503	534	—	29
12	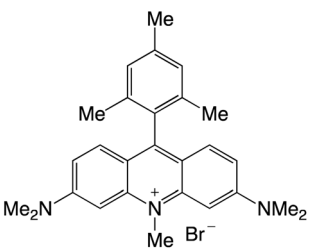	2.40	−1.15	1.25	503	534	2.2	29
13	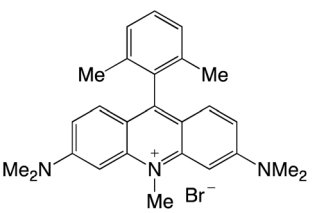	2.40	−1.15	1.25	504	533	—	29

Table 1 (*Contd.*)

Entry	Acridinium based photocatalyst	$E_{0,0}$[a] [eV]	$E_{1/2}$ (C/C^{-})[b] [V *vs.* SCE]	$E_{1/2}$ (C^{*}/C^{-})[c] [V *vs.* SCE]	λ_{abs}[d] [nm] ($\varepsilon \times 10^{3}$ [M^{-1} cm^{-1}])	λ_{em}[e] [nm]	τ[f] [ns]	Ref.
14	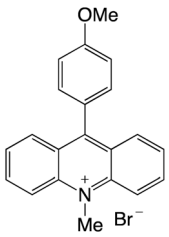	2.77	−0.56	2.21	438	499	—	29
15	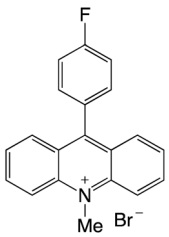	2.83	−0.51	2.32	426	512	—	29
16	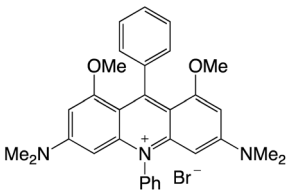	2.40	−1.19	1.21	498	540	4.4	29
17	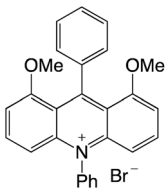	2.23	−0.47	1.76	503	595	3.1	29
18	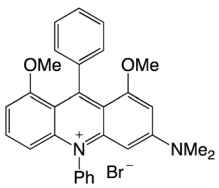	2.25	−0.94	1.31	501	584	4.7	29
19	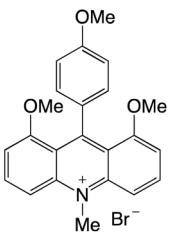	2.30	−0.62	1.68	494	567	5.9	29
20	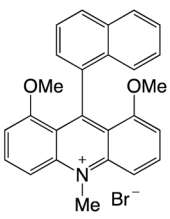	2.39	−0.51	1.88	497	531	4.1	29

Table 1 (*Contd.*)

Entry	Acridinium based photocatalyst	$E_{0,0}$[a] [eV]	$E_{1/2}$ (C/C^{-})[b] [V *vs.* SCE]	$E_{1/2}$ (C^{*}/C^{-})[c] [V *vs.* SCE]	λ_{abs}[d] [nm] ($\varepsilon \times 10^{3}$ [M^{-1} cm^{-1}])	λ_{em}[e] [nm]	τ[f] [ns]	Ref.
21	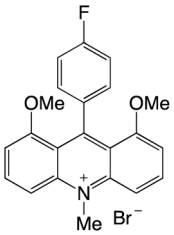	2.31	−0.51	1.80	497	579	3.0	29
22	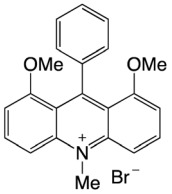	2.33	−0.52	1.81	497	576	2.7	29
23	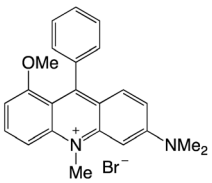	2.30	−0.83	1.47	506	575	0.9, 4.4	29
24	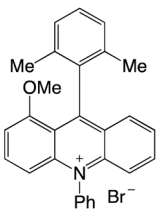	2.25	−0.56	1.69	480	634	1.2, 3.3, 16.8	29
25	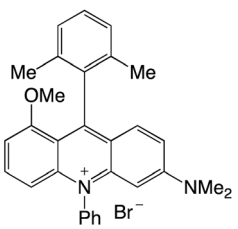	2.29	−0.90	1.39	514	574	1.1, 7.2	29
26	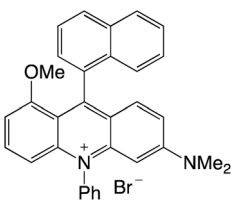	2.27	−0.87	1.40	516	578	1.0, 6.2	29
27	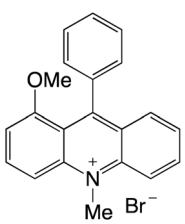	2.29	−0.48	1.81	473	635	1.0, 3.0, 17.3	29

Table 1 (*Contd.*)

Entry	Acridinium based photocatalyst	$E_{0,0}$[a] [eV]	$E_{1/2}$ (C/C^{-})[b] [V *vs.* SCE]	$E_{1/2}$ (C*/C^{-})[c] [V *vs.* SCE]	λ_{abs}[d] [nm] ($\varepsilon \times 10^3$ [M^{-1} cm^{-1}])	λ_{em}[e] [nm]	τ[f] [ns]	Ref.
28	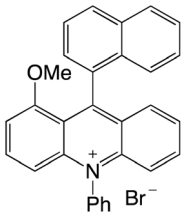	2.26	−0.53	1.73	480	635	1.0, 4.5	29
29	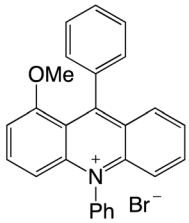	2.23	−0.54	1.69	479	637	1.0, 9.9	29
30	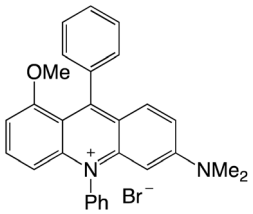	2.29	−0.89	1.40	511	576	1.0, 6.9	29
31	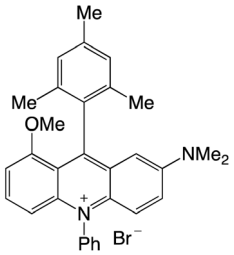	1.94	−0.71	1.23	583	723	1.5, 5.5	29
32	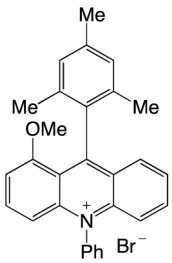	2.25	−0.57	1.68	479	632	1.4, 12.1	29
33	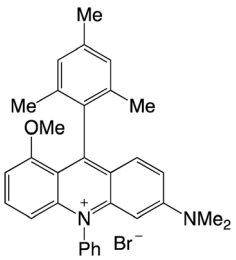	2.29	−0.89	1.40	513	573	1.1, 6.8	29

Table 1 (*Contd.*)

Entry	Acridinium based photocatalyst	$E_{0,0}$[a] [eV]	$E_{1/2}$ (C/C^{-})[b] [V *vs.* SCE]	$E_{1/2}$ (C*/C^{-})[c] [V *vs.* SCE]	λ_{abs}[d] [nm] ($\varepsilon \times 10^3$ [M^{-1} cm^{-1}])	λ_{em}[e] [nm]	τ[f] [ns]	Ref.
34	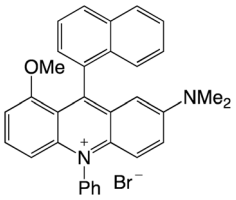	1.87	−0.68	1.19	590	755	0.9, 5.0	29
35	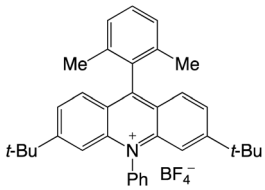	2.67	−0.56	2.11	419	493	16.4	35
36	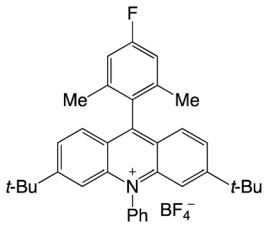	2.67	−0.54	2.13	421	493	16.8	35
37	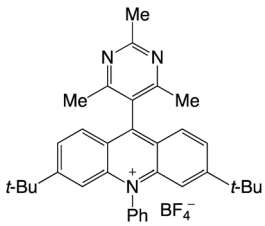	2.63	−0.47	2.16	427	500	16.1	35
38	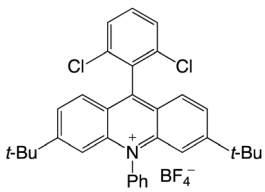	2.64	−0.43	2.21	425	504	17.1	35
39	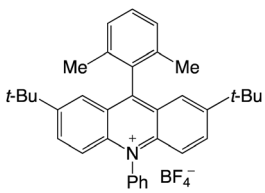	2.62	−0.53	2.09	431	499	19.0	35
40	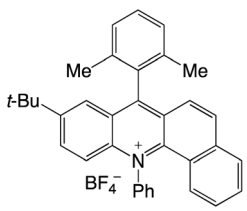	2.60	−0.53	2.07	460	504	0.3, 16.8	35

Table 1 (*Contd.*)

Entry	Acridinium based photocatalyst	$E_{0,0}$[a] [eV]	$E_{1/2}$ (C/C^{-})[b] [V *vs.* SCE]	$E_{1/2}$ (C^{*}/C^{-})[c] [V *vs.* SCE]	λ_{abs}[d] [nm] ($\varepsilon \times 10^{3}$ [M^{-1} cm^{-1}])	λ_{em}[e] [nm]	τ[f] [ns]	Ref.
41	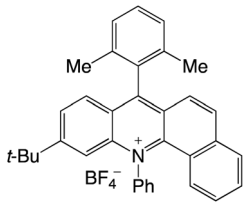	2.60	−0.54	2.06	462	501	0.3, 16.6	35
42	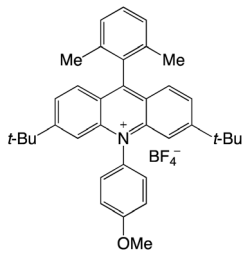	2.63	−0.58	2.05	422	523	1.1, 18.8	35
43	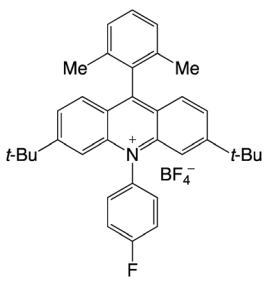	2.66	−0.55	2.11	419	493	17.6	35
44	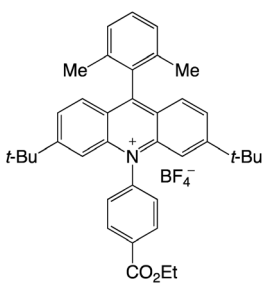	2.66	−0.54	2.12	421	494	18.4	35
45	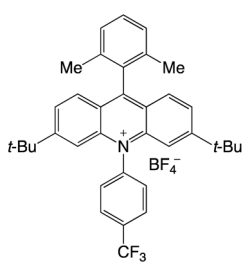	2.65	−0.51	2.14	421	495	20.7	35
46	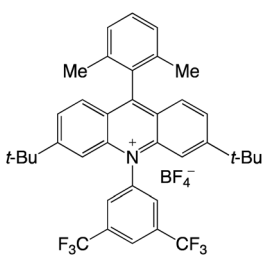	2.64	−0.45	2.19	425	497	20.8	35

Table 1 (*Contd.*)

Entry	Acridinium based photocatalyst	$E_{0,0}$[a] [eV]	$E_{1/2}$ (C/C^{-})[b] [V *vs.* SCE]	$E_{1/2}$ (C^{*}/C^{-})[c] [V *vs.* SCE]	λ_{abs}[d] [nm] ($\varepsilon \times 10^{3}$ [M^{-1} cm^{-1}])	λ_{em}[e] [nm]	τ[f] [ns]	Ref.
47	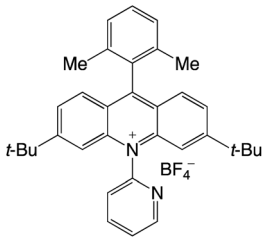	2.67	−0.50	2.17	419	511	2.7, 19.1	35
48	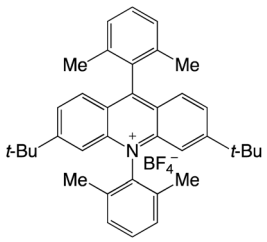	2.67	−0.53	2.14	421	488	22.8	35
49	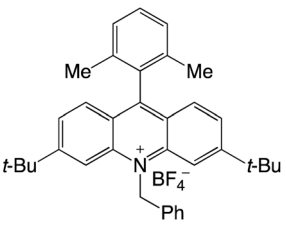	2.67	−0.54	2.13	422	493	23.7	35
50	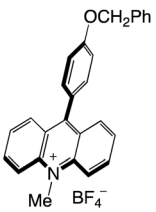	2.46	−0.58	1.88	264, 329, 345, 369, 453	565	6.4	41
51	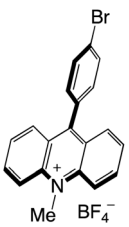	2.61	−0.51	2.10	264, 331, 347, 363, 411, 431, 460	485, 523	8.3	41
52	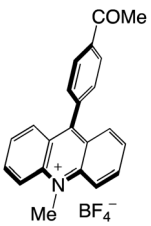	2.60	−0.49	2.11	264, 331, 346, 363, 407, 430, 458	486, 523	14.3	41
53	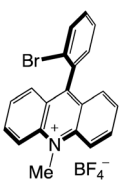	2.65	−0.48	2.17	264, 331, 347, 364, 407, 430, 457	481, 507	16.9	41

Table 1 (*Contd.*)

Entry	Acridinium based photocatalyst	$E_{0,0}$[a] [eV]	$E_{1/2}$ (C/C^{-})[b] [V *vs.* SCE]	$E_{1/2}$ (C^{*}/C^{-})[c] [V *vs.* SCE]	λ_{abs}[d] [nm] ($\varepsilon \times 10^{3}$ [M^{-1} cm^{-1}])	λ_{em}[e] [nm]	τ[f] [ns]	Ref.
54	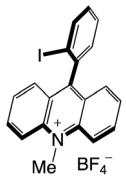	2.63	−0.48	2.15	264, 331, 348, 364, 410, 431, 459	507	<2	41
55	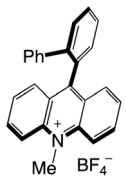	2.61	−0.52	2.09	264, 331, 347, 363, 412, 432, 459	487, 527	7.8	41
56	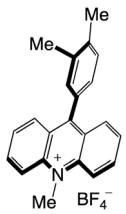	2.59	−0.56	2.03	263, 346, 360, 413, 435, 464	491, 524	<2	41
57	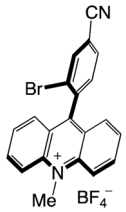	2.64	−0.42	2.22	264, 334, 349, 366, 406, 430, 458	482, 508, 544	19.2	41
58	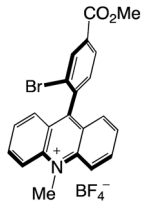	2.65	−0.44	2.21	264, 333, 349, 365, 409, 431, 458	481, 508, 545	18.0	41
59	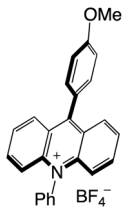	2.45	−0.52	1.93	266, 344, 361, 456	574	6.3	41
60	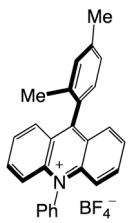	2.63	−0.51	2.12	265, 328, 345, 361, 412, 433, 462	491, 515	10.0	41

Table 1 (*Contd.*)

Entry	Acridinium based photocatalyst	$E_{0,0}$[a] [eV]	$E_{1/2}$ (C/C^{-})[b] [V *vs.* SCE]	$E_{1/2}$ (C^{*}/C^{-})[c] [V *vs.* SCE]	λ_{abs}[d] [nm] ($\varepsilon \times 10^3$ [M^{-1} cm^{-1}])	λ_{em}[e] [nm]	τ[f] [ns]	Ref.
61	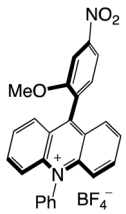	2.62	−0.43	2.19	265, 296, 334, 349, 364, 414, 434, 461	489, 515, 551	12.0	41
62	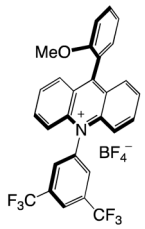	2.38	−0.42	1.96	267, 331, 347, 363, 415, 440, 468	436	6.4	41
63	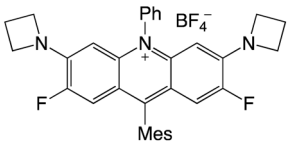	2.40	−0.98	1.42	458–513	494–551	3.7	40
64	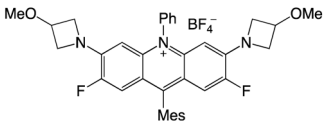	2.42	−0.94	1.48	458–513	494–551	3.4	40
65	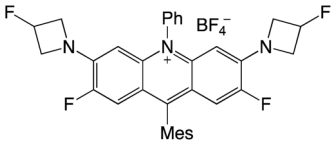	2.45	−0.89	1.56	458–513	494–551	3.4	40
66	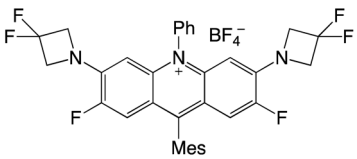	2.50	−0.80	1.70	458–513	494–551	3.2	40
67	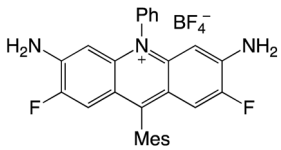	2.63	−0.99	1.64	458–513	494–551	3.9	40
68	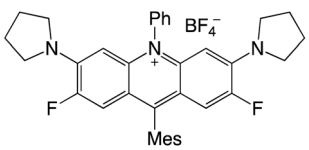	2.37	−0.97	1.40	458–513	494–551	0.6	40
69	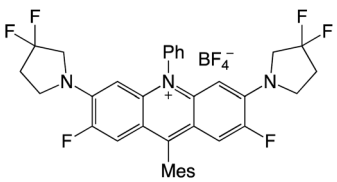	2.48	−0.85	1.61	458–513	494–551	5.1	40

Table 1 (*Contd.*)

Entry	Acridinium based photocatalyst	$E_{0,0}$[a] [eV]	$E_{1/2}$ (C/C$^-$)[b] [V *vs.* SCE]	$E_{1/2}$ (C*/C$^-$)[c] [V *vs.* SCE]	λ_{abs}[d] [nm] ($\varepsilon \times 10^3$ [M^{-1} cm^{-1}])	λ_{em}[e] [nm]	τ[f] [ns]	Ref.
70	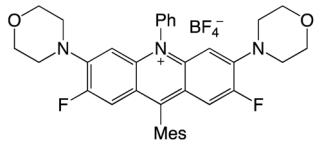	2.38	−0.73	1.65	458–513	494–551	5.4	40
71	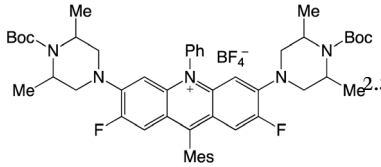	2.37	−0.73	1.64	458–513	494–551	4.7	40
72	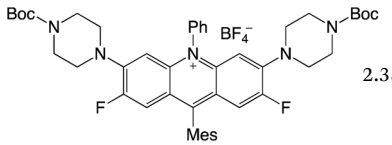	2.38	−0.73	1.65	458–513	494–551	4.3	40
73	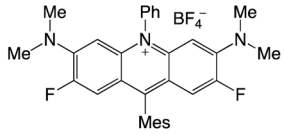	2.39	−0.89	1.50	458–513	494–551	3.1	40
74	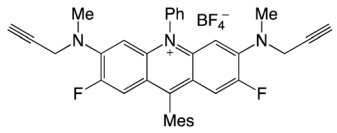	2.46	−0.75	1.71	458–513	494–551	4.4	40
75	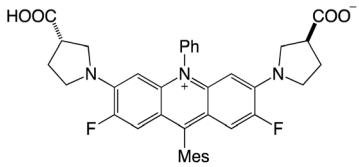	2.37	−1.06	1.31	458–513	494–551	1.4	40
76	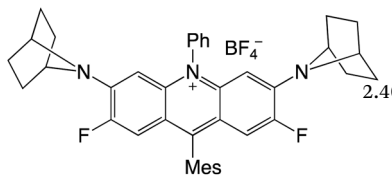	2.40	−0.81	1.59	458–513	494–551	4.2	40
77	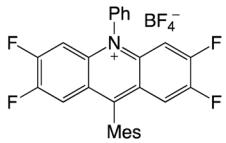	2.35	−0.33	2.02	458–513	494–551	5.9	40
78	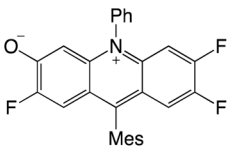	2.35	−1.20	1.51	458–513	494–551	5.4	40
79	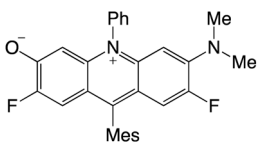	2.40	−1.36	1.03	458–513	494–551	5.02	40

Table 1 (*Contd.*)

Entry	Acridinium based photocatalyst	$E_{0,0}$[a] [eV]	$E_{1/2}$ (C/C^{-})[b] [V *vs.* SCE]	$E_{1/2}$ (C^{*}/C^{-})[c] [V *vs.* SCE]	λ_{abs}[d] [nm] ($\varepsilon \times 10^3$ [M^{-1} cm^{-1}])	λ_{em}[e] [nm]	τ[f] [ns]	Ref.
80	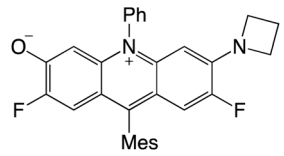	2.42	−1.41	1.01	458–513	494–551	4.8	40
81	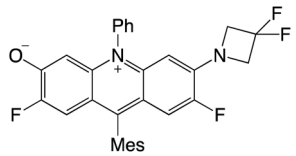	2.40	−1.36	1.03	458–513	494–551	5.4	40

[a] Determined at the intersection between normalized absorption and emission spectra, with $E = 1240/\lambda$. [b] Ground-state reduction potentials determined by cyclic voltammetry (*E vs.* SCE). [c] Excited-state reduction potential, estimated with ground-state reduction potentials and excited-state energies. [d] Conc. ≈ 1.5×10^{-5} M. [e] λ_{em} = 370 nm with ref = quinine sulfate (Φ = 0.546 in H_2SO_4 0.5 M). [f] Time-correlated single-photon counting technique.

A reaction pathway was proposed by Soulé and co-workers[41] (Scheme 4). According to them, upon irradiation of MeAcrH·BF_4, (step 1) generation of the reduced acridinyl radical (step 2) was achieved. Kano *et al.*[42] had earlier reported a comparable synthesis of an acridinyl radical from photoexcited acridinium molecules. The acridinyl radical then effectively reduced all utilized diazonium salts (step 3). These findings support the formation of an aryl radical (step 4) and thermodynamically advantageous electron transfer [−0.2 V < $E_{1/2}$(diazonium/aryl radical) < +0.2 V *vs.* SCE,[43] $E_{1/2}$(acridinium/acridinyl radical)] = −0.54 V *vs.* SCE.[44] The subsequent reaction between the aryl radical and the revived acridinium precursor produced the appropriate acridane species (step 5). Further, DFT calculations supports it's reoxidation into the final product (step 6).

4. Photophysical properties of acridinium-based photocatalysts

Organophotocatalysts offer the chemists for accessing to exotic chemistries and a wide variety of substrates that are typically unreactive in synthetic environments. Furthermore, the variety of these chemical compounds presents a collection that has promise for being helpful in the development and improvement of new synthetic techniques. Table 1 provides information on the photophysical and electrochemical properties of acridinium-based organophotocatalysts.

5. Synthetic applications of acridinium-based photocatalysts

5.1. Amide bond formation

Song *et al.*[45] reported an organic photo-redox catalysed metal, base and additive free amide bond formation. Without harming other functional groups like alcohols, phenols, ethers, esters, halogens, or heterocycles, this green technique demonstrated good functional selectivity.

This technique had a wide substrate range, was well compatible with water, air and had high yields. In this protocol, Song *et al.* has given the synthesis of amide bond formation by reaction between substituted thioacid **1** and primary amine **2** in presence of blue LED under an open air atmosphere (Scheme 5).

The general mechanism for the amide bond formation reaction by photoredox catalyst is proposed by Song *et al.* in Scheme 6. According to this mechanism, intermediate **1A** was generated by deprotonation of thioacid **1** *via* reaction with amine **2**. The blue LED photoexcite [Mes-Acr-$MeBF_4$] to generate excited [Mes-Acr-$MeBF_4$]*, that further reduced to the [Mes-Acr-$MeBF_4$]$^{\bullet}$ radical by electron-rich thioacid anion **1A**. Photocatalysed thioacid anion **1A** generates thioacid radical **1B** *via* single-electron transfer (SET). The diradical coupling of thioacid radical **1B** has given key disulfide **1C** which followed by aminolysis with amine **2** to provide amide **3** and per thioacid

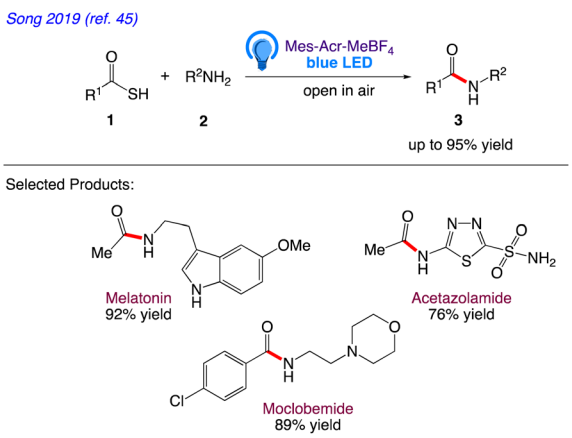

Scheme 5 Acridinium catalyzed amide bond formation.

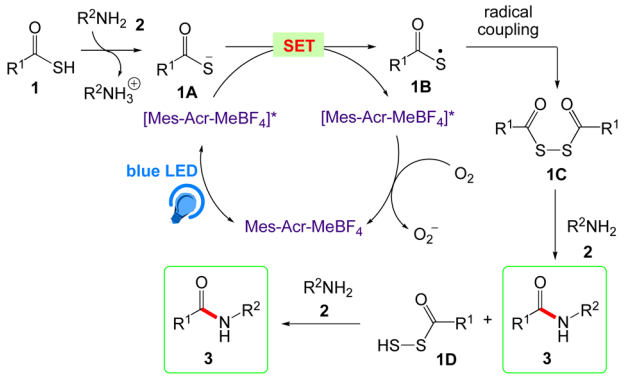

Scheme 6 Proposed mechanism of acridinium catalyzed amide bond formation.

1D. The aminolysis of per thioacid **1D** further results the amide **3**.

5.2. Synthesis of enantioenriched α-deuterated α-amino acids

Wang *et al.* reported[46] a mild, adaptable organophotoredox protocol for the formation of various, enantioenriched, deuterated α-amino acids.

This radical-based approach offers the unrivalled functionality of the convergent unification of readily available feedstock carboxylic acids and a chiral methyleneoxazolidinone fragment as well as the simultaneous highly diastereo, chemo, and regioselective incorporation of deuterium, which could vastly enhance the range of highly valuable deuterated amino acids for biological and medicinal purposes. They hypothesised that by using common, easily accessible alkyl carboxylic acids **4** as radical progenitors, the direct addition of a decarboxylative radical **7** to (*S*)-methyleneoxazolidinone **5** as a chiral inducer might result in enantioenriched amino acids **6** (Scheme 7). The synthesis of more structurally diverse amino acids is made possible by the easy accessibility of feedstock alkyl carboxylic acids **4**. Additionally, researchers hypothesised that the Re-face-selective deuteration of the chiral anion intermediate **9** might offer a new method for creating enantioenriched deuterated amino acids **6**. The simultaneous chemo, regio, and diastereoselective incorporation of large side chains and deuterium into amino acids is anticipated to be the driving force behind the strategy's efficacy.

5.3. Synthesis of quinolin-2(1*H*)-ones from quinoline *N*-oxides

Roy *et al.*[47] reported visible light catalysed an effective, simple procedure for the synthesis of a variety of quinolones and isoquinolones. No stoichiometric reagents are needed for this atom-efficient, environmentally benign protocol without formation of any by products. This very efficient and reagent-free photocatalytic technique involves the reaction of quinoline *N*-oxide **10**, in presence of blue LED. The reaction successfully yielded the desired product **11** with excellent yield at room temperature (Scheme 8).

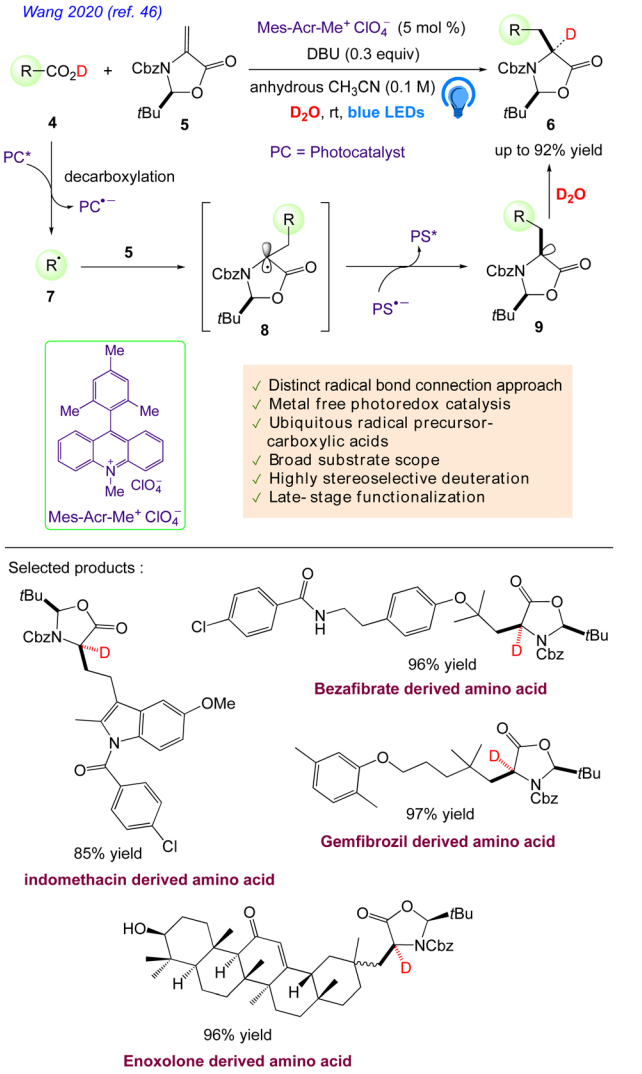

Scheme 7 Synthesis of enantioenriched α-deuterated α-amino acids.

The authors have proposed a SET mechanism as shown in Scheme 9. Single electron donation of *N*-oxide **10** to the HOMO of the photocatalyst from the oxide resulted in a highly unstable

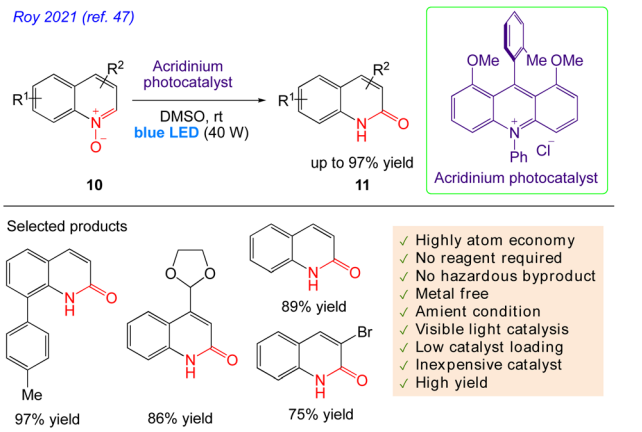

Scheme 8 Synthesis of quinolin-2(1*H*)-ones from quinoline *N*-oxides.

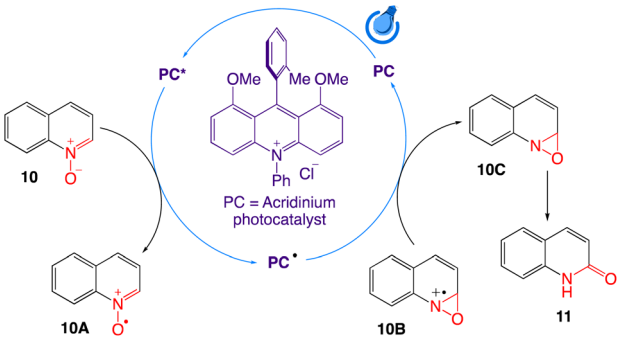

Scheme 9 Proposed mechanism for visible light photoredox catalytic synthesis of quinolin-2(1*H*)-ones.

nucleophilic quinolinium *N*-oxo radical **10A**, which ultimately participates in attacking the vicinal electrophilic C-2 centre to form the kinetically favourable three membered oxaziridine radical cation ring **10B**. The formed radical cation then acts as an acceptor of electrons from the singly occupied LUMO of the photocatalyst to form neutral but relatively unstable oxaziridine **10C**. The weak N–O bond of oxaziridine **10C** finally undergo isomerization to generate stable carbonyls *via* simultaneous hydride migration to generate the corresponding quinolin-2(1*H*)-ones **11** as the final product.

5.4. C–H oxygenation of alkylarenes

Mancheño *et al.*[48] reported a metals and additive free technique for the highly selective, photocatalyzed C–H oxygenation of alkylarenes **12** under air to the corresponding carbonyls **13**. An imide–acridinium, which when exposed to visible light, transforms into a very potent photooxidant, that catalyses the entire reaction. The desired carbonyl compounds were obtained in good yields with excellent chemoselectivity. This process could also be applied to benzyl alcohols and alkylarenes, producing high yields of the related aldehydes and ketones. Different functional groups were tolerated well in both the aldehyde and ketone production processes because of the incredibly mild reaction conditions (Scheme 10).

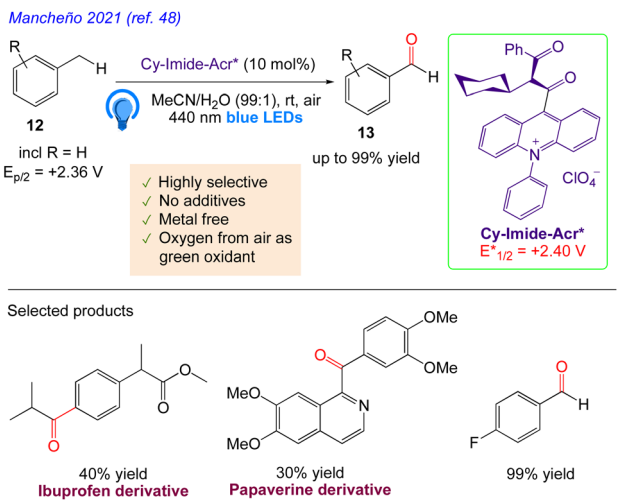

Scheme 10 C–H oxygenation of alkylarenes by photoredox catalysis.

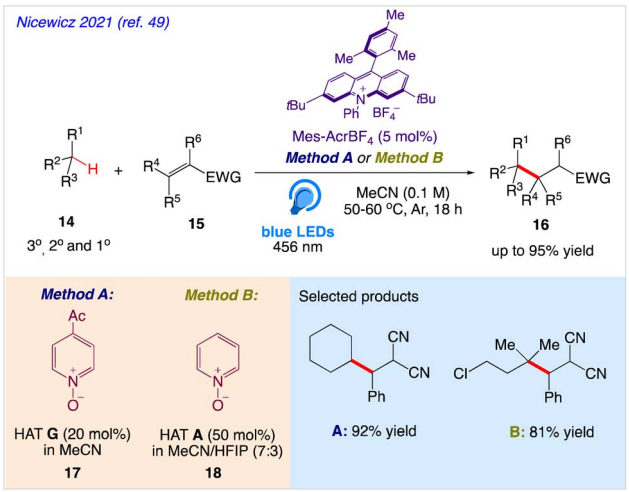

Scheme 11 C–H alkylation reaction using pyridine *N*-oxides as H-atom abstraction agents.

5.5. Aliphatic C–H functionalization using pyridine *N*-oxides as H-atom abstraction agents

Nicewicz *et al.*[49] reported a highly efficient approach for C–H alkylation reactions with the help of a synergistic combination of an acridinium photoredox catalyst and easily accessible pyridine *N*-oxides as HAT precursors. The abstraction of tertiary, secondary, and even powerful primary C–H bonds in the presence of electron donating and electron withdrawing moieties is made possible by this entirely organic method. In this protocol, unactivated tertiary, secondary, and primary C(sp^3)H bonds **14** were successfully alkylated and heteroarylated with electron withdrawing olefins **15** under visible light (Scheme 11). This approach contained key intermediates that can readily have their reactivity changed by making structural changes.

A plausible mechanism was proposed by authors, as depicted in Scheme 12. According to this mechanism, highly

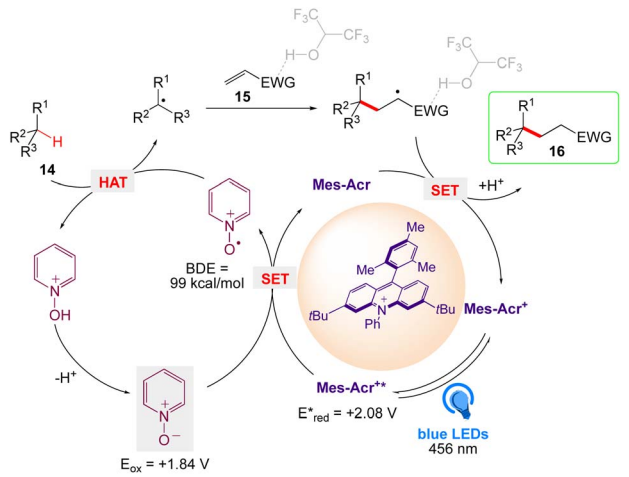

Scheme 12 Proposed mechanism of the C–H alkylation.

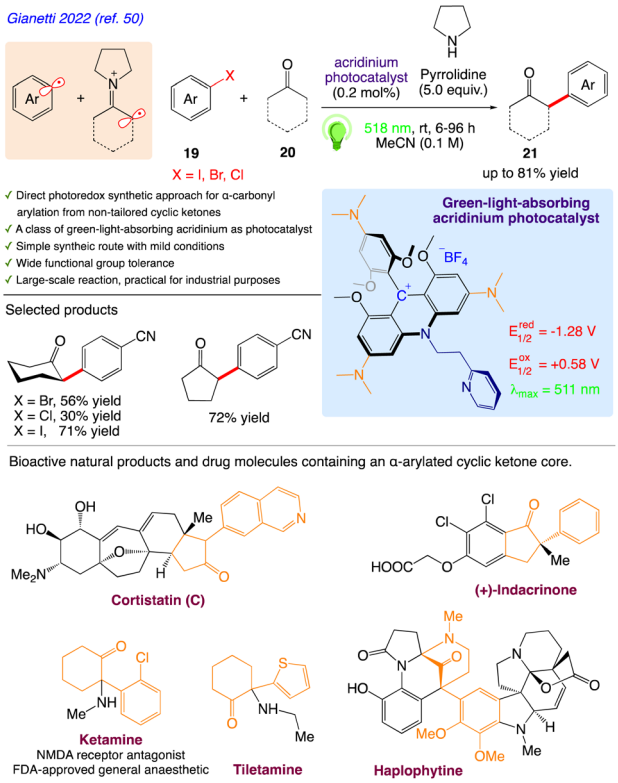

Scheme 13 Photoredox activation for the α-arylation of cyclic ketones.

oxidizing Mes-Acr^{+}* was generated by photoexcitation and pyridine *N*-oxide undergoes SET to become an *N*-oxy radical. A hydrogen atom can be abstracted from a C–H substrate by this electrophilic species (BDE = 99 kcal mol^{-1}), which can subsequently produced an alkyl radical that interacts with an electron-deficient olefin. The resulting electrophilic radical alpha to the EWG was reduced by the acridine radical Mes-Acr followed by protonation from the *N*-hydroxy pyridinium to deliver the C–H alkylated product along with the photoredox catalyst Mes-Acr^{+} and pyridine *N*-oxide, that ultimately closing both the photo and HAT catalytic cycle.

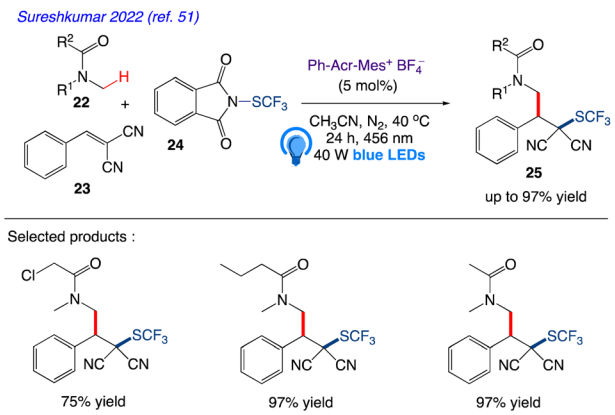

Scheme 14 Multicomponent approach for tandem C(sp^3)–H activation and alkylation followed by trifluoromethylthiolation.

5.6. α-arylation of cyclic ketones

Gianetti *et al.*[50] reported a photocatalytic cycle that activates a C(sp^2)-X bond **19** (X = I, Br, Cl) and α -carbonyl C(sp^3)-H **20** bond to produce ketones **21** from widely available aryl halides. A recently developed photoredox technique for the α-arylation of ketones has illustrated the potential value of this acridinium family. This work develops a metal-free photoredox method for-arylating ketones that is versatile and tolerant of a wide range of functional groups. On a multigram–scale reaction, the transformation has proven to be quite strong and clean. The synthesis of various economically significant building blocks for a wide range of bioactive and pharmacological substances serves as an important illustration of its value (Scheme 13).

5.7. Multicomponent approach for tandem C(sp^3)–H activation and alkylation followed by trifluoromethylthiolation

Sureshkumar *et al.*[51] reported visible light driven one-pot tandem direct C(sp^3)H activation and alkylation followed by trifluoromethylthiolation using an organophotocatalyzed multicomponent method. They presented a tandem, metal-free, three-component method for the photoinduced radical route for the difunctionalization of activated alkenes by utilising 5 equiv. of **22**, 1 equiv of **23**, 1.5 equiv. of "SCF_3" source **24**, acridinium photocatalyst to give the desired product **25** with excellent yield (Scheme 14).

A plausible mechanism was proposed by author as depicted in Scheme 15. According to this mechanism, upon irradiation of organophotocatalyst Ph-Mes-Acr^{+} in presence of a blue LED, excited-state species Ph-Mes-Acr^{+}* is generated, which emits an electron from **22** *via* a single-electron transfer (SET) process to generate the radical cation intermediate **22A** along with the

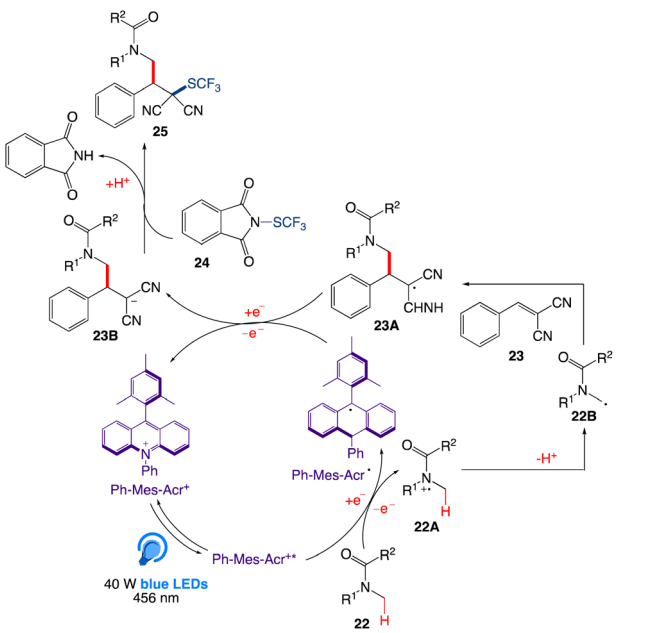

Scheme 15 Plausible reaction mechanism of C(sp^3)–H activation and alkylation followed by trifluoromethylthiolation.

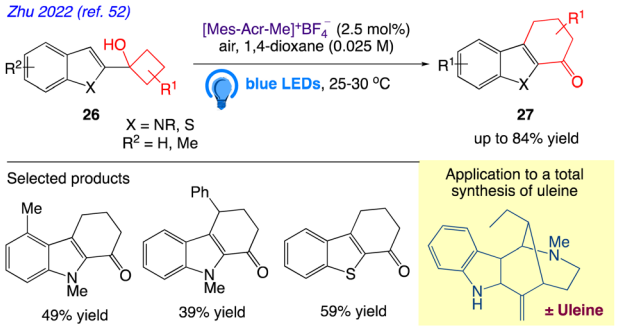

Scheme 16 Two-carbon ring expansion of cyclobutanols to cyclohexenones.

regeneration of Ph-Mes-Acr•. After loosing a proton, intermediate **22A** then generates radical intermediate **22B** that reacts with alkene **23** to generate intermediate **23A**. Intermediate **23A** regenerates photocatalyst Ph-Mes-Acr$^+$ by abstracting one electron from Ph-Mes-Acr•. In the next step, intermediate **23A** is converted to the anionic intermediate **23B**, followed by the trifluoromehylthiolation by **24** to produce the final product **25**.

5.8. Two-carbon ring expansion of cyclobutanols to cyclohexenones

Zhu *et al.*[52] reported visible-light photoredox catalysed an oxidative two-carbon homologation of cyclobutanols **26** to cyclohexenones **27** (Scheme 16). In this present protocol, tetrahydrocarbazol-1-ones with various functionalizations, as well as their thio-analogues, were easily produced from the commonly available 1-(1*H*-indol-2-yl)cyclobutan-1-ols and 1-(benzo[*b*]thiophen-2-yl)cyclobutan-1-ols owing to the reaction's broad substrate range. Subsequently, a straightforward complete synthesis of (±)-uleine that incorporates this two-carbon ring expansion step was developed.

A plausible mechanism, proposed by author is depicted in Scheme 17. According to this mechanism a SET oxidation of indole **26** *via* the excited acridinium salt to radical cation **26A**, produced benzylic radical **26B** through a pinacol rearrangement. A second SET from **26B** to either MesAcr$^+$* afforded the benzylic cation **26C**, which further undergo a Wagner–Meerwein 1,2-alkyl shift to afforded cation **26D**. Finally, a rearomatization of **26D** has given product **27** and oxidation of

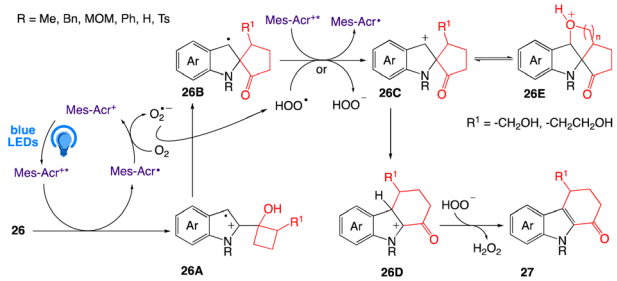

Scheme 17 Proposed mechanism of two-carbon ring expansion of cyclobutanols to cyclohexenones.

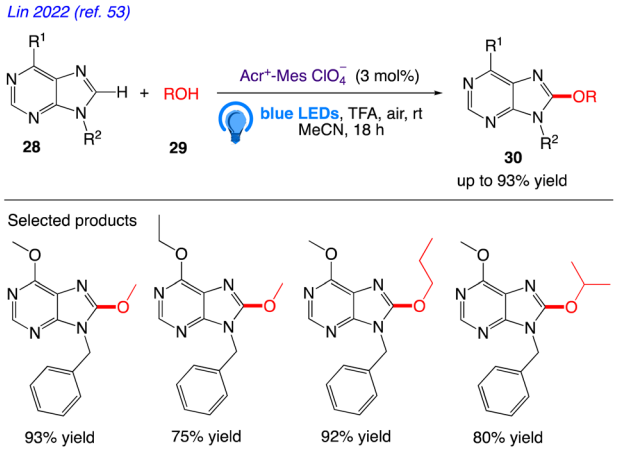

Scheme 18 Synthesis of C8 alkoxylated purine derivatives.

MesAcr• by oxygen to MesAcr$^+$ complete the photoredox catalytic cycle.

5.9. Purine C8 alkoxylation with alcohol

Lin *et al.*[53] reported the visible light mediated and acridinium catalysed cross-dehydrogenation coupling reaction between purines **28** and alcohols **29** to synthesise a number of C8-alkoxy purine derivatives **30**, under an air atmosphere, which served as the only oxidant in the reaction (Scheme 18). With good to excellent yields, these mild reaction conditions provide a wide variety of C8-alkoxylated compounds.

The plausible mechanism as proposed by authors are depicted in Scheme 19. According to this mechanism, The Acr$^+$-Mes ClO_4^- photocatalyst is converted into it's excited [Acr$^+$-Mes ClO_4^-]* *via* irradiation of blue LEDs. Further, the excited state *via* a single electron transfer (SET) process with **28** generates the purine radical cation **28A** and the Acr-Mes radical. The Acr-Mes radical is then oxidized by O_2 and completes the photocatalytic cycle. The alcohol (ROH) **29** and purine radical cation **28A** reacts to generate the alkoxide adduct radical **28B**. Subsequently, **28B** undergoes an SET process with HOO• and generates

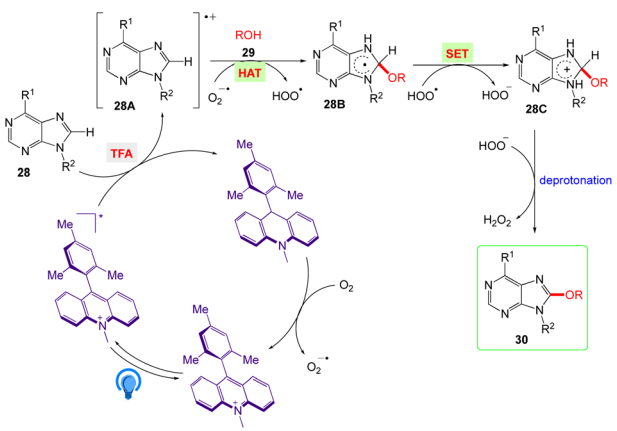

Scheme 19 Proposed reaction mechanism of synthesis of C8 alkoxylated purine derivatives.

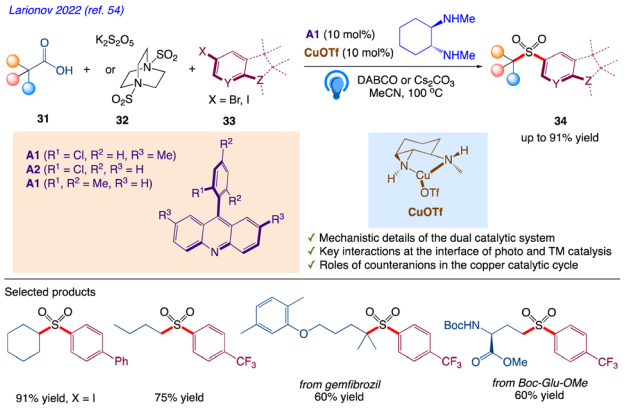

Scheme 20 Tricomponent decarboxysulfonylative cross-coupling with aryl halides.

intermediate **28C**. Finally, deprotonation of **28C** yields the target product **30**, and HOO^- acquires the proton to give H_2O_2.

5.10. Tricomponent decarboxysulfonylative cross-coupling with aryl halides

Larionov *et al.*[54] reported a visible light-induced, dual catalytic, direct decarboxysulfonylative cross-coupling of carboxylic acids with aryl halides. This reaction includes tricomponent decarboxysulfonylative cross-coupling of carboxylic acid **31** with aryl iodide **33** occurs readily in the dual catalytic system of acridine photocatalyst and diamine ligated copper(I) triflate, with DABCO or potassium metabisulfite **32** that results sulfone **34** with 91% yield (Scheme 20).

The plausible mechanism as proposed by author is depicted in Scheme 21. According to the mechanism, sulfonyl radical generates sulfinic acid *via* hydrogen abstraction from the acridinyl radical **31B**, emerging from the photoinduced PCET-enabled decarboxylation in complex **31A** (path A, Scheme 21). The base-mediated anion exchange then converts Cu^I complex **33A** to sulfinate intermediate **32A** that undergo an oxidative addition with an aryl halide *via* intermediate **32B**, followed by reductive elimination, giving rise to the sulfone product in an overall orthogonal relay dual catalytic process. Acridinyl radical-mediated formation of Cu^0 species can also enable an alternative mechanism for the aromatic decarboxysulfonylation that proceeds through an oxidative addition of the aryl halide to the Cu^0 intermediate, producing arylcopper species **33B** (path B, Scheme 21). The copper intermediate **32B** is produced by further cross-termination with the sulfonyl radical, and the sulfone product is then produced by reductive elimination.

5.11. Cross-coupling arylation

Rueping *et al.*[55] reported a synthetic protocol for the site-specific arylation of ketones **37** from tertiary alcohols **35** and 4-bromoacetophenone **36** *via* photoredox-enabled MS-PCET and nickel catalysis (Scheme 22).

The plausible mechanism as proposed by author is depicted in Scheme 23. According to the mechanism, upon irradiation

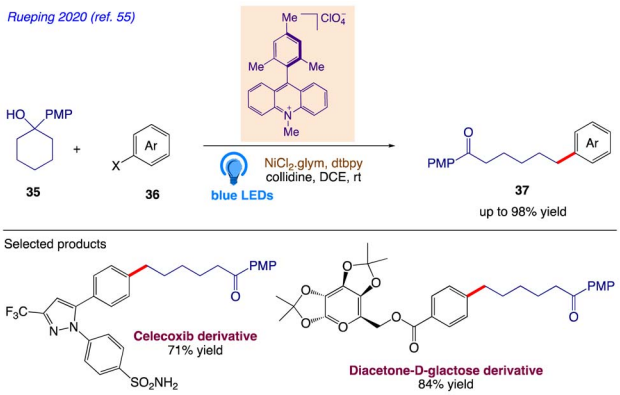

Scheme 22 Arylation of ketones from easily accessible tertiary alcohols through a photoredox-enabled MS-PCET and nickel catalysis.

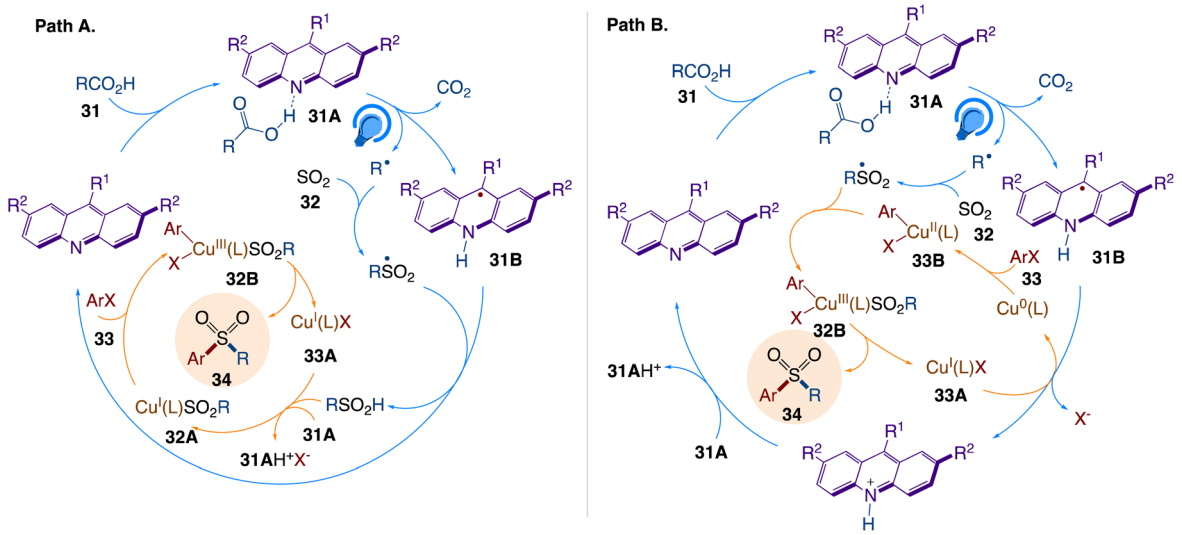

Scheme 21 Mechanistic pathways of the dual catalytic decarboxysulfonylation.

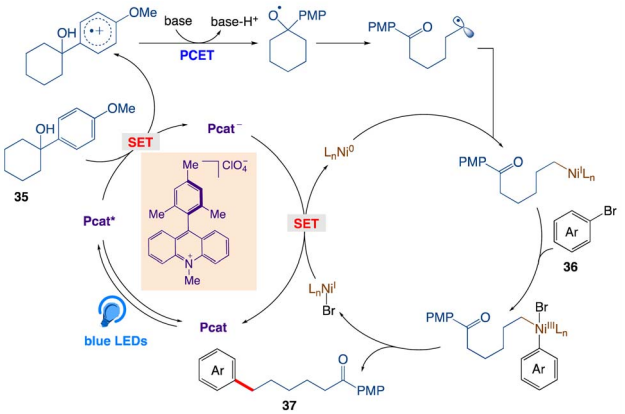

Scheme 23 Proposed mechanism for C–C activation/cross coupling.

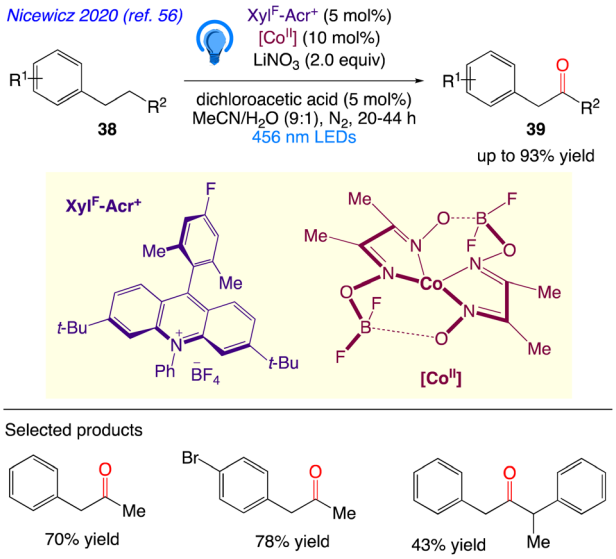

Scheme 24 Site-selective homobenzylic oxidation.

with visible light, the ground-state of Mes-Acr-Me$^+$ is promoted to its highly oxidizing singlet excited state *Mes-Acr-Me$^+$, followed by a single electron transfer with the tertiary alcohol **35**, furnishing the corresponding arene radical cation along with the reduced form of the photocatalyst Mes-Acr-Me$^\bullet$. Subsequent deprotonation (PT) and intramolecular ET reaction between the alkoxide and the radical cation gives the key alkoxyl radical species, which readily cleaves into a carbonyl moiety and a distal carbon-centered radical through scission of the neighboring C–C bond at the β position. The alkyl radical is then captured by the Ni(0) and gives an alkylnickel(I) intermediate, which rapidly undergo oxidative addition with an aryl halide, generating a Ni(III) species. The cross-coupled product and the Ni(I) intermediate are then produced by reductive elimination at this point; the latter can be reduced by the reduced form of the photocatalyst and regenerate both at once, completing the catalytic cycle.

5.12. Homobenzylic oxygenation

Nicewicz *et al.*[56] reported protocol for the selective oxidation of typically inert C–H bonds. In this synthetic protocol, they demonstrated that utilising a combination of dual organic photoredox and cobalt catalysis, it is possible to utilize of the reactivity of benzylic C(sp^3)H bonds at the homobenzylic site. In a two-part catalytic system, alkyl arenes **38** are dehydrogenated, followed by an anti-Markovnikov Wacker-type oxidation, to produce benzyl ketone **39** products (Scheme 24).

A plausible mechanism, as proposed by authors is depicted in Scheme 25. According to this mechanism, initial oxidation of the nitrate anion ($Ep_{p/2}{}^{ox} = +1.97$ V) results from the excited state photooxidant, **Xyl^F-Acr$^+$*** ($E^*_{red} = +2.13$ V). The resulting nitrate radical is a potent H-atom abstracting agent, allowing it to excise the weak C(sp^3)–H bond of **38** generating HNO_3 and benzylic radical **38A**. **Xyl^F-Acr$^\bullet$** ($E_{1/2}{}^{ox} = -0.54$ V) can feasibly undergo single electron transfer (SET) with [Co^{II}] ($E_{1/2}{}^{red} = -0.51$ V) to regenerate **Xyl^F-Acr$^+$** and a reduced cobalt complex (*vide infra*). [Co^I]$^-$ likely undergoes protonation to form [Co^{III}]–H assisted by the aforementioned acid additive. **38A** is then intercepted by [Co^{III}]–H, liberating H_2 and **38B**. One possibility of this mechanism is the direct protonation of [Co^{III}]–H. This would form [Co^{III}]$^+$ ($E_{1/2}{}^{red} \sim +0.2$ V), which could potentially oxidize **38A** ($E_{1/2}{}^{ox} \sim +0.37$ V). While this SET is endergonic by about +0.2 V (4.6 kcal mol^{-1}), rapid deprotonation of the resulting benzylic cation intermediate would render SET irreversible, ultimately generating styrene **38B**. Alternatively two molecules of [Co^{III}]–H could undergo a bimolecular reductive elimination of H_2 generating two equivalents of [Co^{II}]. **38B** would then be formed *via* the addition of **38A** to [Co^{II}], forming a putative [Co^{III}] alkyl intermediate capable of undergoing a net β-hydride elimination. **38B** can then engage in a second catalytic cycle to form the olefin radical cation (**38C**) whereupon trapping with water would afford a distonic radical cation (**38D**). Subsequent deprotonation and a second dehydrogenation would furnish the desired product **39** *via* a sequence similar to the mechanisms proposed by Lei and Nicewicz.

5.13. Synthesis of alkene-containing *N*-heterocycles

Liu *et al.*[57] reported a synthetic protocol for radical azacyclization of α-imino-oxy acids **40** with pendant alkenes **41** and **42** *via* synergistic photoredox and cobaloxime catalysis (Scheme 26). With the fusion of cobalt catalysis and photoredox organocatalysis, they devised the iminyl-radical-mediated cyclization technique.

The plausible mechanism as proposed by author is depicted in Scheme 27. According to this mechanism, initial step involves a single oxidation of the carboxylate derived from the α-imino-oxy acid **40** and base by Mes-Acr$^+$*, generating an iminyl radical **40A** with loss of CO_2 and acetone, followed by 5-*exo* cyclization to deliver an alkyl radical **40B**. The reduced photocatalyst Mes-Acr$^\bullet$ could be single-electron oxidized by a Co^{III} complex to close the photoredox catalytic cycle, as well as the generation of a Co^{II} complex. Similarly, the alkyl radical **40B** can react with the Co^{II} complex to form an organocobalt(III) complex **40C**. The critical β-H elimination step readily occurs to furnish

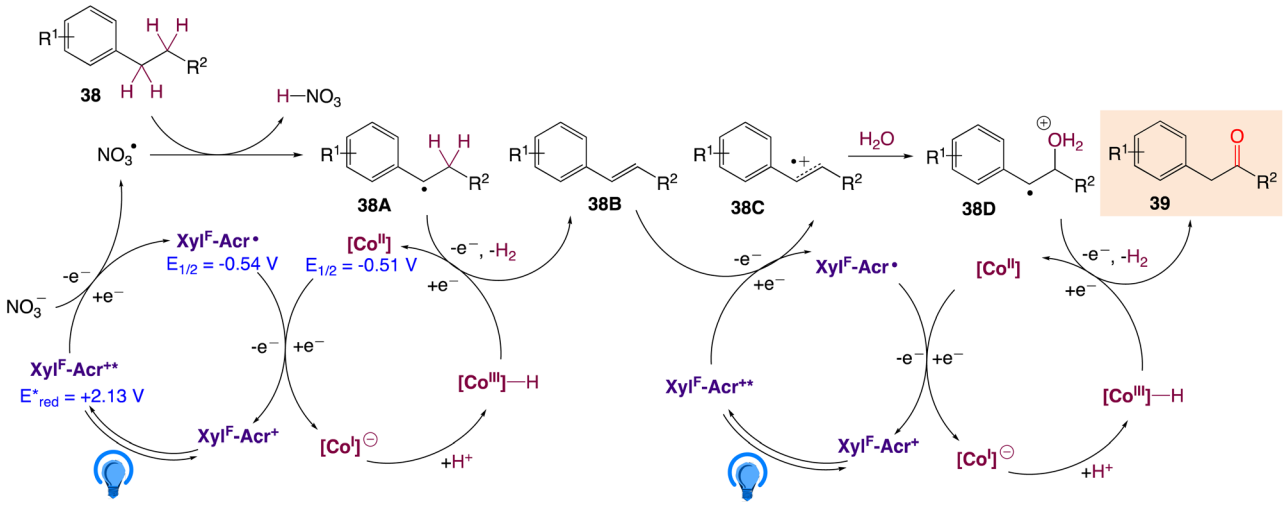

Scheme 25 Mechanistic proposal for $LiNO_3$-mediated homobenzylic oxidation.

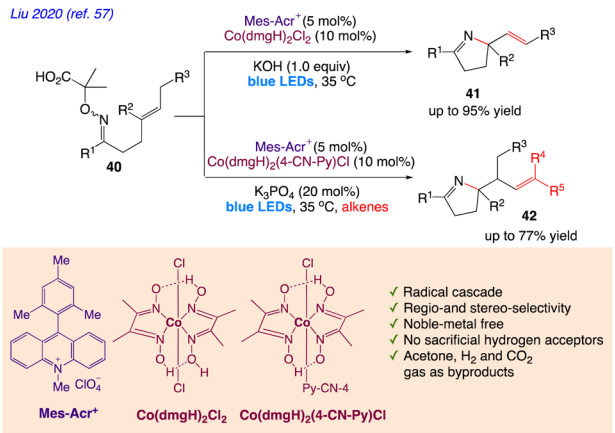

Scheme 26 Radical aza-cyclization of α-imino-oxy acids for synthesis of alkene-containing *N*-heterocycles.

the Heck-type product **41** and a Co^{III}–H intermediate. The reaction of the Co^{III}–H complex with a proton leads to H_2 extrusion and completion of the cobalt catalytic cycle.

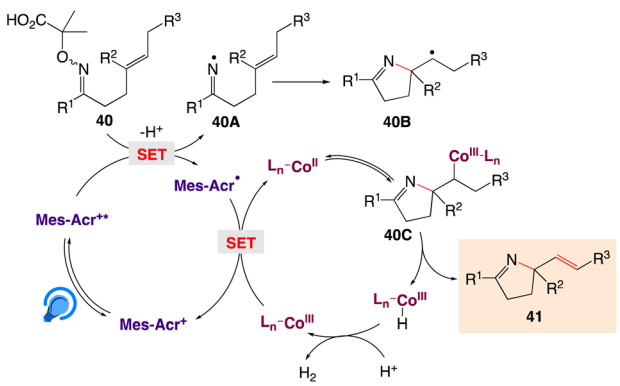

Scheme 27 Proposed Mechanism for synthesis of alkene-containing *N*-heterocycles.

5.14. Regiospecific synthesis of distally unsaturated ketones with hydrogen evolution

Wu *et al.*[58] reported a photoredox/cobalt dual catalytic system for the synthesis of distally unsaturated ketones **44** from dehydrogenation of nonstrained tertiary cycloalkanols **43** using the dual catalyst system of photosensitizer Mes-2,7-Me_2-Acr-Me^+ and cobaloxime catalyst $Co(dmgH)_2Py_2OTf$ under visible-light irradiation (Scheme 28).

The plausible mechanism as proposed by author is depicted in Scheme 29. According to this mechanism, visible-light-excitation of Mes-2,7-Me_2-Acr-Me^+ followed by SET with *para*-methoxyphenyl group of the tertiary alcohol **43** gave rise to the corresponding arene radical cation intermediate **43A** along with the reduced form of the photocatalyst Mes-2,7-Me_2-Acr-$Me^•$. This reduced photocatalyst Mes-2,7-Me_2-Acr-$Me^•$ further oxidized by the Co^{III} catalyst to regenerate the photocatalyst and generates Co^{II}. In presence of an exogenous Bronsted base alkoxyl radical **43B** is generated by subsequent intramolecular PCET between the arene radical cation **43A** and the adjacent hydroxyl group, which undergoes C–C bond β-scission to form

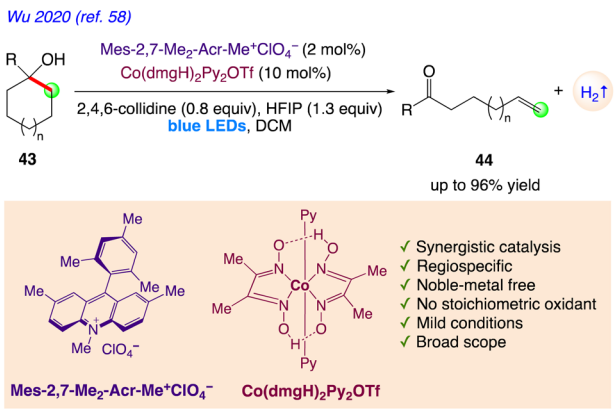

Scheme 28 Regiospecific synthesis of distally unsaturated ketones with hydrogen evolution.

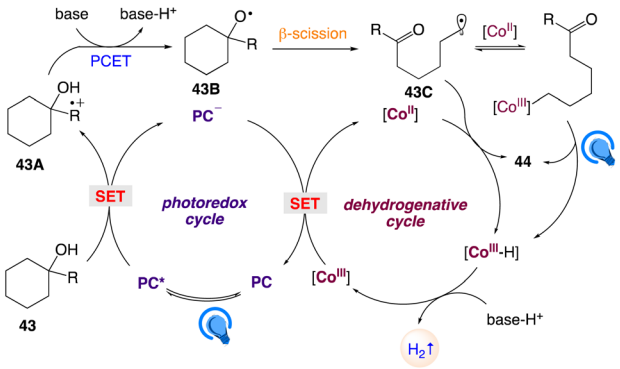

Scheme 29 Proposed reaction mechanism for regiospecific synthesis of distally unsaturated ketones with hydrogen evolution.

the ring-opened distal-carbonyl alkyl radical **43C**. The alkyl radical **43C** is then trapped by the Co^{II} species to give an alkyl–Co^{III} intermediate, which undergoes photoinduced homolytic cleavage of the Co–C bond followed by β-H abstraction *via* Co^{II} to gives a Co^{III} hydride and the desired product **44**. On the other hand, a direct HAT on the alkyl radical **43C** by Co^{II}, without the intermediacy of alkyl–Co^{III}, cannot be excluded. Protonation of the Co^{III} hydride emits H_2 and regenerates the Co^{III} catalyst to complete the cycle.

5.15. Functional group-divergent decarboxysulfonylation by acridine photocatalysis

Larionov *et al.*[59] reported a photocatalytic system for direct decarboxylative conversion of carboxylic acids **45** to sulfones **46** and sulfinates **47**, as well as sulfonyl chlorides **48** and fluorides **49** in single step and in a multicomponent fashion (Scheme 30).

This synthetic protocol includes visible light-induced, organophotocatalytic reaction which includes conversion into sulfones, sulfinates, sulfonyl chlorides, and sulfonyl fluorides *via* direct tricomponent decarboxylative coupling of carboxylic acids.

5.16. Reductive elimination

Iwasawa *et al.*[60] reported a 4-phosphinoacridine ligands catalysed synthetic protocol for visible-light-induced transition-metal catalysis and developed a Pd-catalyzed cross-coupling reaction of aryl halides **50** with carboxylic acids **51** under irradiation with blue LEDs to give the aryl esters **52** (Scheme 31).

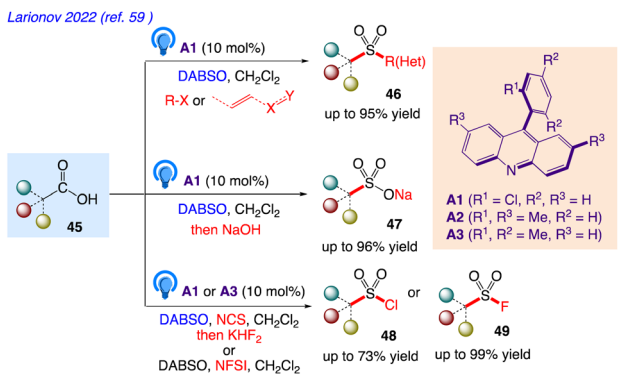

Scheme 30 Functional group-divergent decarboxysulfonylation by acridine photocatalysis.

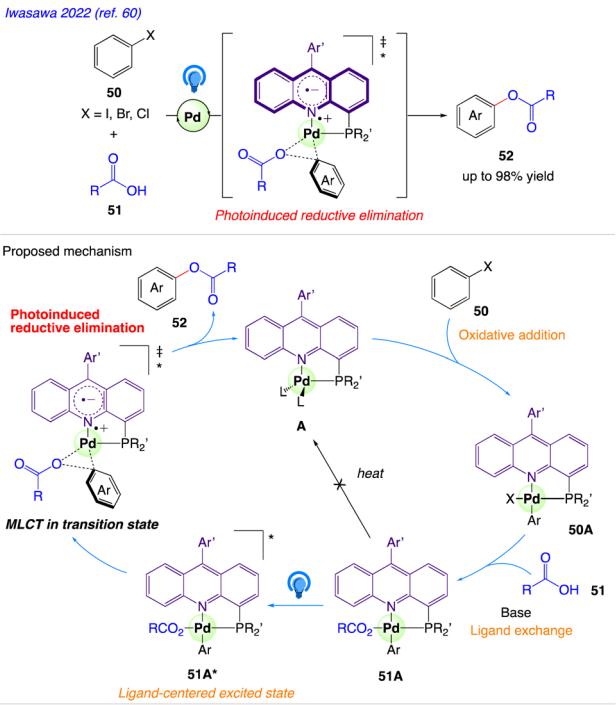

Scheme 31 Proposed Mechanism for acridine–Pd-catalyzed cross-coupling of aryl halides with carboxylic acids.

The plausible mechanism as proposed by author is depicted in Scheme 31. According to this mechanism, Pd(0) complex **A** undergoes oxidative addition of an aryl halide **50** to give ArPd(II) X complex **50A**, which reacts with carboxylic acids **51** and further converted to $ArPd(II)O_2CR$ complex **51A** *via* ligand exchange. Complex **51A** is excited by visible light to form an acridine-centered excited state **51A*** in T1, which undergoes reductive elimination of an aryl ester **52** and regenerate **A**. This step is assisted by an MLCT (metal to ligand charge transfer) character of the transition state in the excited state.

5.17. Alkyl radical generation *via* C–C bond cleavage in 2-substituted oxazolidines

Under photoredox catalysed conditions, Fagnoni *et al.*[61] reported a class of easily synthesised uncharged precursors for the quick release of alkyl radicals (tertiary, α-oxy, and α-amido). Using photo-organoredox catalysis, in presence of a commercially available and widely employed organic dye ($Acr\text{-}Mes^+BF_4^-$) as the photoredox catalyst, 2-substituted-1,3-oxazolidines **53** have been successfully used to these radicals in alkylation of olefins **54** to give the desired alkylated product **55**.

The plausible mechanism as proposed by author is depicted in Scheme 32. According to this mechanism, compound **53** is radical precursor and the monoelectronic oxidation of **53** by the photoexcited acridinium catalyst $Acr\text{-}Mes^{+}$* gives the corresponding radical cation **53A**.

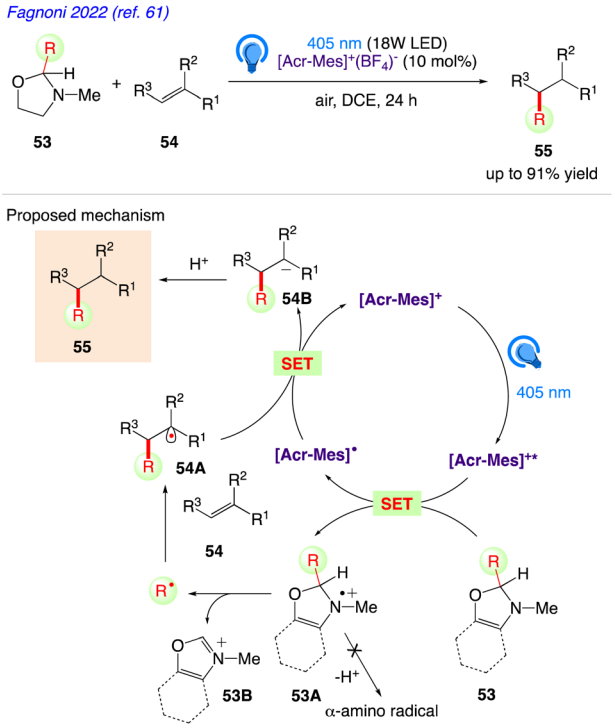

Scheme 32 Proposed Mechanism for alkyl radical generation *via* C–C bond cleavage in 2-substituted oxazolidines.

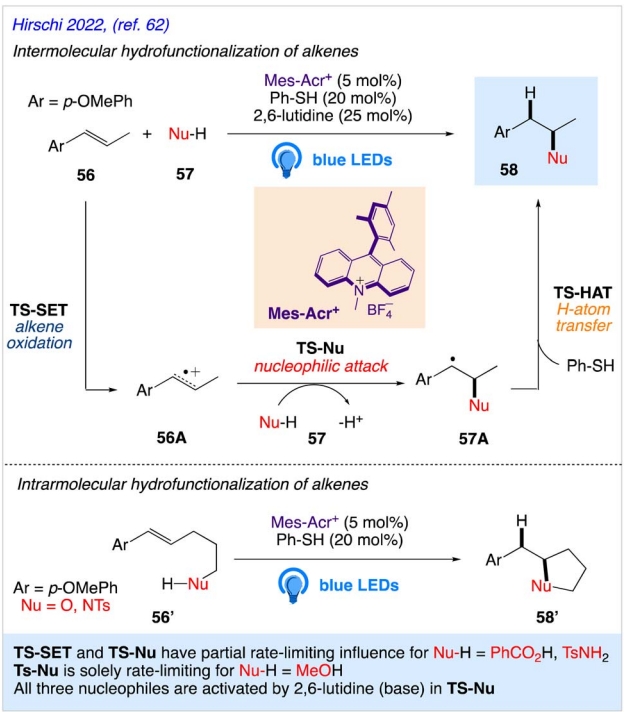

Scheme 33 Acridinium catalyzed anti-markovnikov hydrofunctionalization of alkenes.

At this step, an unprecedented C–C cleavage takes place in **53A**, releasing a carbon-centered radical and a stable iminium ion **53B**. The unique structure of the oxazolidines prevents potential α-deprotonation from positions 2 and 4 as well as from the *N*-Me group to give a α-amino radical during the radical cation stage. The alkyl radicals are in turn, trapped by electron-poor olefins or vinyl (hetero)aromatics **54** to give adduct radical **54C**. Back electron transfer from Acr-Mes• to the adduct radical **54C** followed by protonation gave the desired alkylated product **55** followed by restoring the photoredox catalyst.

5.18. Anti-Markovnikov hydrofunctionalization of alkenes

Nicewicz group have reported both intermolecular and intramolecular alkene hydrofunctionalization reactions utilizing acridinium salts as photocatalysts. Hirschi *et al.*[62] reported a mechanistic evaluation of intermolecular alkene hydrofunctionalization reactions for the same. They proposed the mechanism of the intermolecular hydrofunctionalization using model alkene (anethole) **56** that undergo oxidation *via* single electron transfer (SET) by a photoexcited acridinium catalyst (Mes-Acr^{+}*) to form cation radical intermediate **56A** and the reduced acridine radical Mes-Acr•. Further, it is followed by attack of the nucleophile (Nu-H) **57**, resulting in the generation of carbon-centered radical intermediate **57A**. H-atom transfer (HAT) from the thiol co-catalyst to **57A** afforded the anti-Markovnikov product **58** (Scheme 33). Qualitative evidence for rate-limiting nucleophilic attack in all three reactions is provided by a typical ^{13}C KIE on the olefinic carbon that is subject to nucleophilic assault.

5.19. Synthesis of *gem*-fluorophosphonate alkenes

Bonnaire *et al.*[63] reported an effective method for synthesizing fluorovinylphosphonates using acridinium photocatalysis in moderate and metal-free conditions. In this synthetic protocol, in presence of Fukuzumi's catalyst (9-mesityl-10-methylacridinium perchlorate), *gem*-bromo fluoroalkenes **59** have been coupled with phosphite **60** to produce valuable *gem*-fluorophosphonate derivatives **61** (Scheme 34). The intended products were produced in yields that ranged from good to excellent, and the reaction exhibited high chemical stability.

5.20. Photocatalytic decarboxylative pyridylation of carboxylic acids

Through radical-mediated decarboxylation and the simultaneous inclusion of pyridyl groups, Hong *et al.*[64] reported a highly potent catalytic system for visible-light-induced reactions using *N*-amidopyridinium salts **62** and diverse carboxylic acids **63** to give the desired pyridine based organic compound **64** (Scheme 35). Due to the prevalence and abundance of

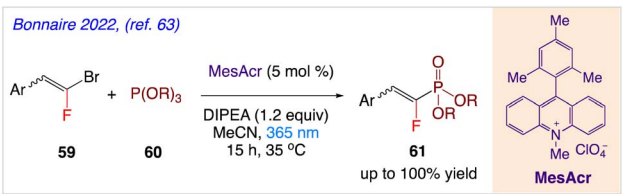

Scheme 34 Synthesis of *gem*-fluorophosphonate alkenes.

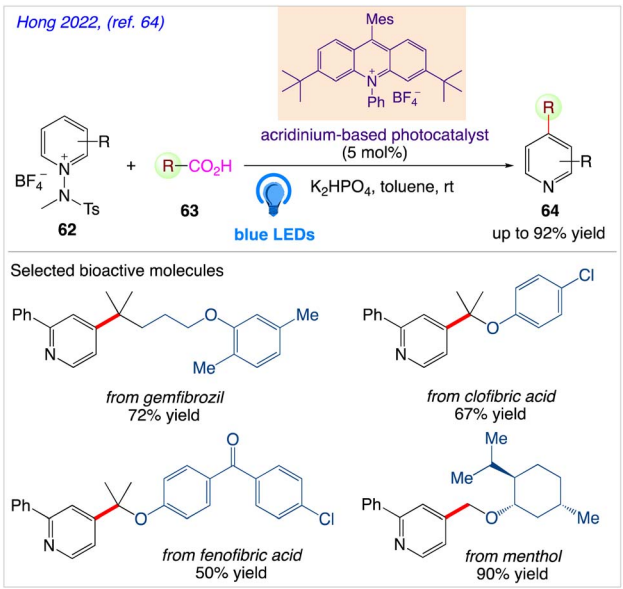

Scheme 35 Photocatalytic decarboxylative pyridylation of carboxylic acids.

carboxylic acids, they anticipated that this catalytic system can directly enable the C–H pyridylation of carboxylic acids upto a greater amount as well as scope of its wide spread applicability in synthetic and therapeutic chemistry.

The plausible mechanism as proposed by author is depicted in Scheme 36. According to this mechanism, the carboxylate, generated under basic conditions, undergoes SET with the excited state of Mes-Acr$^+$ in presence of visible light. The generated carboxylic radical generates the alkyl radical *via* decarboxylation, which is assured for radical addition at the C4 position of the *N*-amidopyridinium salt **62**. Intermediate **62A** undergoes facile deprotonation and homolytic cleavage to furnish amidyl radical **62B**. Furthermore, the desired product **64** is generated, with the *in situ*-generated *N*-centered amidyl radical **62B** regenerating the photocatalyst *via* direct SET.

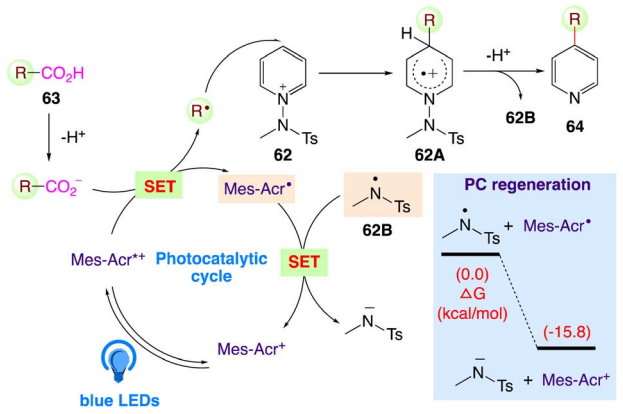

Scheme 36 Proposed reaction mechanism for photocatalytic decarboxylative pyridylation of carboxylic acids.

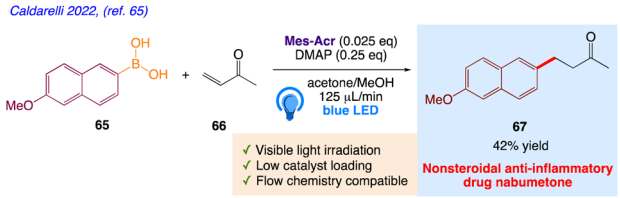

Scheme 37 Acridinium-based photocatalyst in the Giese-type coupling of arylboronic acids with electron poor olefins (synthesis of nabumetone).

5.21. Giese-type coupling of arylboronic acids with electron poor olefins (synthesis of nabumetone)

Caldarelli *et al.*[65] reported the synthetic protocol involving arylboronic acids **65** with different methyl vinyl ketone **66** to give the desired product nabumetone **67** in a Giese-type reaction under photochemical conditions (Scheme 37). This protocol utilizes use of inexpensive metal-free photocatalysts and DMAP as a Lewis base activator with broader and an easy set-up. This reaction process has been used to create a straightforward anti-inflammatory medication and can be executed in-batch or in-flow.

5.22. Acridine radical photoreductant induced organic transformations

Nicewicz and co-workers[66] repored the *in situ* generation of acridine radical that may act as a potent single-electron reductant produced by single-electron reduction of an acridinium derivative upon excitation with 390 nm light. In addition to enhancing the well-known oxidative chemistry associated with acridinium salts, the development of chemoselective dehalogenation reaction carried out from aryl halide **68** to give the desired substituted aryl compound **69** and detosylation reaction including tosylated amine derivatives **70** were smoothly converted to the desired free amines using Mes-Acr$^•$. This protocol also highlights the potential for the development of a variety of reactions based on the excitation of organic radicals.

The plausible mechanism as proposed by author is depicted in Scheme 38. According to this mechanism, upon excitation, Mes-Acr$^+$BF$_4^-$ engages in single electron transfer with the tertiary amine reductant DIPEA, generating Mes-Acr$^•$ and the corresponding amine cation radical. Mes-Acr$^•$, which is then excited by 390 nm light and undergoes electron transfer with an electronically matched aryl halide, producing an arene radical anion and regenerating Mes-Acr$^+$BF$_4^-$. The aryl radical is produced as a result of the splitting of arene radical anion. The resultant aryl radical extracts a hydrogen atom from the amine cation radical, producing the desired product as well as the corresponding iminium salt.

5.23. Excited-state acridine radicals catalysed ketone–olefin coupling of aliphatic and aromatic carbonyls

Nicewicz and co-workers[67] described a mild, metal-free ketone–olefin coupling reaction using an excited-state acridine

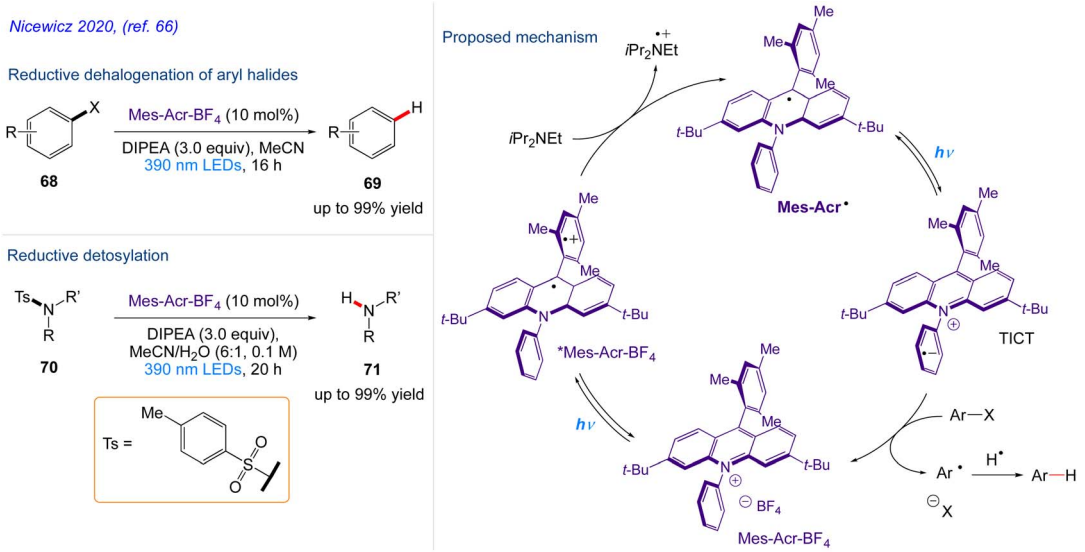

Scheme 38 Acridine radical photoreductant induced organic transformations.

radical super reductant as a photoredox catalyst. They demonstrated both intramolecular and intermolecular ketone–olefin couplings of aliphatic and aromatic ketones and aldehydes **72** to give the desired cycloadduct **73**.

The plausible mechanism as proposed by author is depicted in Scheme 39. According to this mechanism, If "ketone first" reduction is operative, a ketyl radical **72A** is formed, which can undergo a radical 5-*exo*-trig cyclization with the corresponding olefin to provide a carbon-centered radical **72C**. Then, terminal HAT can occur to give the corresponding cyclized product **73**. Alternatively, when "olefin first" reduction occurs, they proposed that the olefin radical anion **72B** formed, can undergo a two-electron attack at the carbonyl to generate **72C**. Subsequent HAT from either DIPEA or 1,4-CHD can trap out the corresponding cycloadduct **73**.

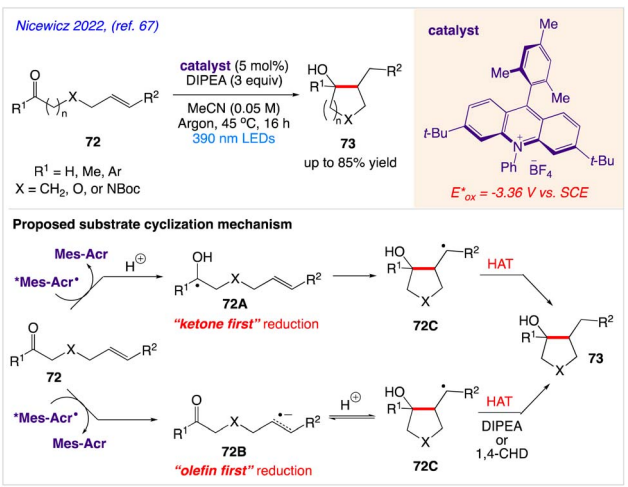

Scheme 39 Excited-state acridine radicals catalysed ketone–olefin coupling of aliphatic and aromatic carbonyls.

5.24. Nucleophilic aromatic substitution of unactivated fluoroarenes

Nicewicz and co-workers[68] proposed a method for the cation radical-accelerated nucleophilic aromatic substitution, which enables for the nucleophilic defluorination of inactive

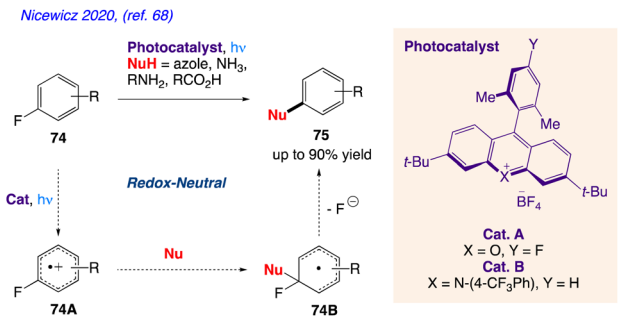

Scheme 40 Nucleophilic aromatic substitution of unactivated fluoroarenes.

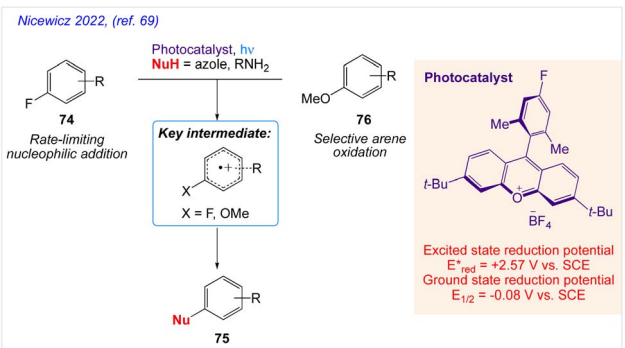

Scheme 41 Mechanistic investigations into amination of unactivated arenes *via* cation radical accelerated nucleophilic aromatic substitution.

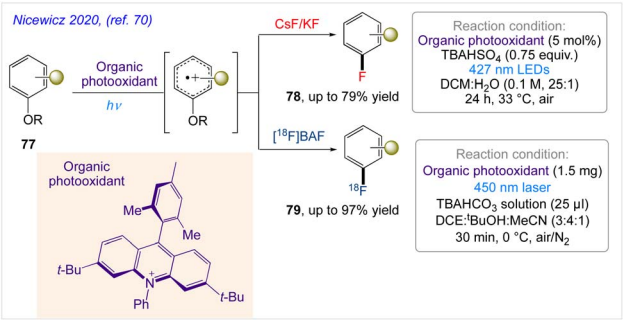

Scheme 42 ^{19}F- and ^{18}F–arene deoxyfluorination *via* organic photoredox-catalysed polarity-reversed nucleophilic aromatic substitution.

fluoroarenes. Under benign conditions, this method can be rendered easy to use by application of organic photoredox catalysis and is suitable for a variety of nucleophile classes, including azoles, amines, and carboxylic acids. Using this technique, specific fluorinated heterocycles can be functionalized. The functionalization of pharmaceuticals in its late stages is also described. The organic transformation, as proposed by them has been represent in Scheme 40 indicating nucleophilic substitution of fluoroarenes **74** desired compound **75** *via* intermediate **74A** and **74B**.

Further, Nicewicz and co-workers[69] also reported mechanistic investigations into site-selective arene amination of unactivated arenes *via* cation radical accelerated nucleophilic aromatic substitution (Scheme 41).

5.25. ^{19}F- and ^{18}F–arene deoxyfluorination

Nicewicz and co-workers[70] demonstrated a polarity-reversed photoredox-catalysed arene deoxyfluorination that operates throughcation-radical-accelerated aromatic nucleophilic substitution that enables the fluorination of electron-rich arenes with ^{19}F– and ^{18}F– under mild conditions. In this protocol, selective (radio)fluorination of electron-rich arenes with CsF or KF and [^{18}F]TBAF has obtained under mild conditions(Scheme 42).

6. Conclusions

A considerable number of acridinium catalysts have been developed in recent years and applied in a variety of visible-light photocatalytic reactions. This made it possible to tailor the redox attributes to a range that most suited for photosynthetic procedures. Recent advances in synthetic chemistry have made it possible to access a variety of photocatalysts with flexible photophysical and electrochemical properties, leading to new reactivities including the functionalization of inert bonds and late stage synthetic applications. In this review, recent applications of acridine in organic synthesis are discussed. As a result, we think that, the field of acridinium based organophotocatalysis will develop, that open up a new avenue for investigation and certainly it has a bright future ahead of it.

Conflicts of interest

"There are no conflicts to declare".

References

1 J. M. R. Narayanam and C. R. J. Stephenson, *Chem. Soc. Rev.*, 2011, **40**, 102–113.
2 J. Twilton, C. Le, P. Zhang, M. H. Shaw, R. W. Evans and D. W. C. MacMillan, *Nat. Rev. Chem.*, 2017, **1**, 0052.
3 N. A. Romero and D. A. Nicewicz, *Chem. Rev.*, 2016, **116**, 10075–10166.
4 C. S. Wang, P. H. Dixneuf and J. F. Soul, *Chem. Rev.*, 2018, **118**, 7532–7585.
5 A. Wimmer and B. Konig, *Beilstein J. Org. Chem.*, 2018, **14**, 54–83.
6 J. Chen, Y. Li, L. Mei and H. Wu, *Chin. J. Org. Chem.*, 2019, **39**, 3040–3050.
7 Y. Chen, L. Q. Lu, D. G. Yu, C. J. Zhu and W. J. Xiao, *Sci. China Chem.*, 2019, **62**, 24–57.
8 L. Marzo, K. Pagire, O. Reiser and B. Konig, *Angew. Chem., Int. Ed.*, 2018, **57**, 10034–10072.
9 T. P. Nicholls, D. Leonori and A. C. Bissember, *Nat. Prod. Rep.*, 2016, **33**, 1248–1254.
10 Z. Zhang, J. H. Ye, T. Ju, L. L. Liao, H. Huang, Y. Y. Gui, W. J. Zhou and D. G. Yu, *ACS Catal.*, 2020, **10**, 10871–10885.
11 F. F. Tan, X. Y. He, W. F. Tian and Y. Li, *Nat. Commun.*, 2020, **11**, 6126.
12 G. Ciamician, *Science*, 1912, **36**, 385–394.
13 (*a*) J. Eberhard, K. Peuntinger, R. Fröhlich, D. M. Guldi and J. Mattay, *Eur. J. Org. Chem.*, 2018, 2682–2700; (*b*) A. Gini, M. Uygur, T. Rigotti, J. Alemán and O. García Mancheño, *Chem. – Eur. J.*, 2018, **24**, 12509–12514; (*c*) K. Durka, M. Urban, M. Dabrowski, P. Jankowski, T. Klis and S. Luliński, *ACS Omega*, 2019, **4**, 2482–2492; (*d*) A. Tlili and S. Lakhdar, *Angew. Chem., Int. Ed.*, 2021, **60**, 19526–19549.
14 D. P. Haria and B. Konig, *Chem. Commun.*, 2014, **50**, 6688–6699.
15 J. B. Metternich and R. Gilmour, *J. Am. Chem. Soc.*, 2015, **137**, 11254–11257.
16 J. J. Molloy, T. Morack and R. Gilmour, *Angew. Chem., Int. Ed.*, 2019, **58**, 13654–13664.
17 J. J. Molloy, T. Morack and R. Gilmour, *Angew. Chem.*, 2019, **131**, 13789–13800.
18 (*a*) Y. Lee and M. S. Kwon, *Eur. J. Org. Chem.*, 2020, **2020**, 6028–6043; (*b*) K. C. Cartwright, S. B. Lang and J. A. Tunge, *J. Org. Chem.*, 2019, **84**, 2933–2940; (*c*) F. F. Tan, X. Y. He, W. F. Tian and Y. Li, *Nat. Commun.*, 2020, **11**, 6126; (*d*) Y. X. Cao, G. Zhu, Y. Li, N. L. Breton, C. Gourlaouen, S. Choua, J. Boixel, H. P. J. Rouville and J. F. Soulé, *J. Am. Chem. Soc.*, 2022, **144**, 5902–5909; (*e*) K. C. Cartwright, S. B. Lang and J. A. Tunge, *J. Org. Chem.*, 2019, **84**(5), 2933–2940.
19 A. Vega-Pecaloza, J. Mateos, X. Companyó, M. Escudero-Casao and L. Dell'Amico, *Angew. Chem., Int. Ed.*, 2021, **60**, 1082–1097.

20 (*a*) S. Fukuzumi, H. Kotani, K. Ohkubo, S. Ogo, N. V. Tkachenko and H. Lemmetyinen, *J. Am. Chem. Soc.*, 2004, **126**, 1600–1601; (*b*) Y. C. Lin and C. T. Chen, *Org. Lett.*, 2009, **11**, 4858–4861; (*c*) C. Fischer, C. Kerzig, B. Zilate, O. S. Wenger and C. Sparr, *ACS Catal.*, 2019, **10**, 210–215; (*d*) S. Fukuzumi, K. Ohkubo, T. Suenobu, K. Kato, M. Fujitsuka and O. Ito, *J. Am. Chem. Soc.*, 2001, **123**, 8459–8467.

21 (*a*) K. Ohkubo, K. Mizushima, R. Iwata, K. Souma, N. Suzuki and S. Fukuzumi, *Chem. Commun.*, 2010, **46**, 601–603; (*b*) I. A. MacKenzie, L. Wang, N. P. R. Onuska, O. F. Williams, K. Begam, A. M. Moran, B. D. Dunietz and D. A. Nicewicz, *Nature*, 2020, **580**, 76–80; (*c*) H. Yan, J. Song, S. Zhu and H. C. Xu, *CCS Chem.*, 2021, **3**, 317–325.

22 L. Marzo, S. K. Pagire, O. Reiser and B. Konig, *Angew. Chem., Int. Ed.*, 2018, **57**, 10034–10072.

23 C. Zhu, H. Yue, L. Chu and M. Rueping, *Chem. Sci.*, 2020, **11**, 4051–4064.

24 K. L. Skubi, T. R. Blum and T. P. Yoon, Dual catalysis strategies in photochemical synthesis, *Chem. Rev.*, 2016, **116**, 10035–10074.

25 (*a*) J. Twilton, C. Le, P. Zhang, M. H. Shaw, R. W. Evans and D. W. C. MacMillan, *Nat. Rev. Chem.*, 2017, **1**, 0052; (*b*) S. Reischauer and B. Pieber, *iScience*, 2021, **24**, 102209.

26 (*a*) A. Y. Chan, I. B. Perry, N. B. Bissonnette, B. F. Buksh, G. A. Edwards, L. I. Frye, O. L. Garry, M. N. Lavagnino, B. X. Li, Y. Liang, E. Mao, A. Millet, J. V. Oakley, N. L. Reed, H. A. Sakai, C. P. Seath and D. W. C. MacMillan, *Chem. Rev.*, 2022, **122**(2), 1485–1542; (*b*) J. Twilton, C. Le, P. Zhang, M. H. Shaw, R. W. Evans and D. W. C. MacMillan, *Nat. Rev. Chem.*, 2017, **1**, 0052.

27 (*a*) C. Zhu, H. Yue, L. Chu and M. Rueping, *Chem. Sci.*, 2020, **11**, 4051–4064; (*b*) V. T. Nguyen, V. D. Nguyen, G. C. Haug, H. T. Dang, S. Jin, Z. Li, C. F. Hansen, B. S. Benavides, H. D. Arman and O. V. Larionov, *ACS Catal.*, 2019, **9**, 9485–9498.

28 C. Fischer, C. Kerzig, B. Zilate, O. S. Wenger and C. Sparr, *ACS Catal.*, 2020, **10**, 210–215.

29 B. Zilate, C. Fischer and C. Sparr, *Chem. Commun.*, 2020, **56**, 1767–1775.

30 (*a*) V. Srivastava, P. K. Singh and P. P. Singh, *Croat. Chem. Acta*, 2014, **87**, 91–95; (*b*) V. Srivastava, P. K. Singh and P. P. Singh, *Chem. Heterocycl. Compd.*, 2014, **50**, 573–578; (*c*) V. Srivastava, P. K. Singh and P. P. Singh, *Croat. Chem. Acta*, 2015, **88**, 59–65; (*d*) V. Srivastava, P. K. Singh and P. P. Singh, *Croat. Chem. Acta*, 2015, **88**, 227–233; (*e*) V. Srivastava, P. K. Singh and P. P. Singh, *Asian J. Chem.*, 2016, **28**, 2159–2163; (*f*) V. Srivastava, P. K. Singh and P. P. Singh, *Rev. Roum. Chim.*, 2016, **61**, 755–761; (*g*) V. Srivastava, P. K. Singh and P. P. Singh, *Croat. Chem. Acta*, 2017, **90**, 435–441; (*h*) V. Srivastava, P. K. Singh, S. Kanaujia and P. P. Singh, *New J. Chem.*, 2018, **42**, 688; (*i*) P. K. Singh, P. P. Singh and V. Srivastava, *Croat. Chem. Acta*, 2018, **91**, 383–387; (*j*) V. Srivastava, P. K. Singh and P. P. Singh, *Tetrahedron Lett.*, 2019, **60**, 40–43; (*k*) V. Srivastava, P. K. Singh and P. P. Singh, *Tetrahedron Lett.*, 2019, **60**, 1333–1336; (*l*) V. Srivastava, P. K. Singh and P. P. Singh, *Tetrahedron Lett.*, 2019, **60**, 151041; (*m*) V. Srivastava, P. K. Singh and P. P. Singh, *Rev. Roum. Chim.*, 2020, **65**, 221–226; (*n*) S. Tivari, P. K. Singh, P. P. Singh and V. Srivastava, *RSC Adv.*, 2022, **12**, 35221; (*o*) M. Mishra, V. Srivastava, P. K. Singh and P. P. Singh, *Croat. Chem. Acta*, 2022, **95**(1), 25–30; (*p*) M. Z. Beg, P. K. Singh, P. P. Singh and V. Srivastava, *Mol. Diversity*, 2023, DOI: 10.1007/s11030-022-10595-2; (*q*) S. P. Singh, V. Srivastava, P. K. Singh and P. P. Singh, *Tetrahedron*, 2023, **132**, 133245.

31 (*a*) V. Srivastava and P. P. Singh, *RSC Adv.*, 2017, **7**, 31377–31392; (*b*) V. Srivastava, P. K. Singh, A. Srivastava and P. P. Singh, *RSC Adv.*, 2020, **10**, 20046; (*c*) A. Srivastava, P. K. Singh, A. Ali, P. P. Singh and V. Srivastava, *RSC Adv.*, 2020, **10**, 39495; (*d*) V. Srivastava, P. K. Singh, A. Srivastava and P. P. Singh, *RSC Adv.*, 2021, **11**, 14251–14259; (*e*) V. Srivastava and P. P. Singh, *Org. Biomol. Chem.*, 2021, **19**, 313–321; (*f*) P. P. Singh, P. K. Singh, M. Z. Beg, A. Kashyap and V. Srivastava, *Synth. Commun.*, 2021, **51**, 3033–3058; (*g*) V. Srivastava, P. K. Singh, A. Srivastava, S. Sinha and P. P. Singh, *Photochem*, 2021, **1**, 237–246; (*h*) V. Srivastava, P. K. Singh, S. Tivari and P. P. Singh, *Org. Chem. Front.*, 2022, **9**, 1485; (*i*) V. Srivastava, P. K. Singh and P. P. Singh, *J. Photochem. Photobiol. C*, 2022, **50**, 100488; (*j*) V. Srivastava and P. P. Singh, *RSC Adv.*, 2022, **12**, 18245; (*k*) P. P. Singh, S. Sinha, G. Pandey and V. Srivastava, *RSC Adv.*, 2022, **12**, 29826; (*l*) P. P. Singh, P. K. Singh and V. Srivastava, *Org. Chem. Front.*, 2023, **10**, 216.

32 C. K. Prier, D. A. Rankic and D. W. C. MacMillan, *Chem. Rev.*, 2013, **113**, 5322–5363.

33 J. M. R. Narayanam and C. R. J. Stephenson, *Chem. Soc. Rev.*, 2011, **40**, 102–113.

34 T. P. Yoon, M. A. Ischay and J. Du, *Nat. Chem.*, 2010, **2**, 527–532.

35 (*a*) A. Gini, M. Uygur, T. Rigotti, J. Alemán and O. G. Mancheño, *Chem. – Eur. J.*, 2018, **24**, 12509–12514; (*b*) A. R. White, L. Wang and D. A. Nicewicz, *Synlett.*, 2019, **30**, 827–832.

36 H. Kotani, K. Ohkubo and S. J. Fukuzumi, *J. Am. Chem. Soc.*, 2004, **126**, 15999–16006.

37 A. Joshi-Pangu, F. Lévesque, H. G. Roth, S. F. Oliver, L. C. Campeau, D. Nicewicz and D. A. DiRocco, *J. Org. Chem.*, 2016, **81**, 7244–7249.

38 C. Fischer and C. Sparr, *Angew. Chem., Int. Ed.*, 2018, **57**, 2436.

39 C. Fischer and C. Sparr, *Tetrahedron*, 2018, **74**, 5486.

40 V. Hutskalova and C. Sparr, *Org. Lett.*, 2021, **23**, 5143–5147.

41 Y. X. Cao, G. Zhu, Y. Li, N. L. Breton, C. Gourlaouen, S. Choua, J. Boixel, H. P. J. Rouville and J. F. Soulé, *J. Am. Chem. Soc.*, 2022, **144**, 5902–5909.

42 K. Kano, B. Zhou and S. Hashimoto, *Bull. Chem. Soc. Jpn.*, 1987, **60**, 1041–1047.

43 P. Allongue, M. Delamar, B. Desbat, O. Fagebaume, R. Hitmi, J. Pinson and J. M. Savéant, *J. Am. Chem. Soc.*, 1997, **119**, 201–207.

44 N. W. Koper, S. A. Jonker, J. W. Verhoeven and C. van Dijk, *Recl. Trav. Chim. Pays-Bas*, 1985, **104**, 296–302.

45 W. Song, K. Dong and M. Li, *Org. Lett.*, 2020, **22**, 371–375.
46 P. Ji, Y. Zhang, Y. Dong, H. Huang, Y. Wei and W. Wang, *Org. Lett.*, 2020, **22**, 1557–1562.
47 S. Mandal, S. Bhuyan, S. Jana, J. Hossain, K. Chhetria and B. G. Roy, *Green Chem.*, 2021, **23**, 5049.
48 M. Uygur, J. H. Kuhlmann, M. C. Pérez-Aguilar, D. G. Piekarski and O. G. Mancheño, *Green Chem.*, 2021, **23**, 3392.
49 M. Schlegel, S. Qian and D. A. Nicewicz, *ACS Catal.*, 2020, **12**, 10499–10505.
50 M. M. Hossain, A. C. Shaikh, J. Moutet and T. L. Gianetti, *Nat. Synth.*, 2022, **1**, 147–157.
51 K. G. Ghosh, D. Das, S. Garai, P. Chandu and D. Sureshkumar, *J. Org. Chem.*, 2022, **87**, 8611–8622.
52 A. Leclair, Q. Wang and J. Zhu, *ACS Catal.*, 2022, **12**, 1209–1215.
53 Z. Luo, C. Lu, G. Histand and D. Lin, *J. Org. Chem.*, 2022, **87**, 11558–11564.
54 V. D. Nguyen, R. Trevino, S. G. Greco, H. D. Arman and O. V. Larionov, *ACS Catal.*, 2022, **12**, 8729–8739.
55 L. Huang, T. Ji and M. Rueping, *J. Am. Chem. Soc.*, 2020, **142**, 3532–3539.
56 J. B. McManus, J. D. Griffin, A. R. White and D. A. Nicewicz, *J. Am. Chem. Soc.*, 2020, **142**, 10325–10330.
57 J. L. Tu, J. L. Liu, W. Tang, M. Su and F. Liu, *Org. Lett.*, 2020, **22**, 1222–1226.
58 X. Wang, Y. Li and X. Wu, *ACS Catal.*, 2022, **12**, 3710–3718.
59 V. T. Nguyen, G. C. Haug, V. D. Nguyen, N. T. H. Vuong, G. B. Karki, H. D. Armana and O. V. Larionov, *Chem. Sci.*, 2022, **13**, 4170.
60 N. Toriumi, T. Inoue and N. Iwasawa, *J. Am. Chem. Soc.*, 2022, **144**, 19592–19602.
61 A. L. Ruiz, M. L. Mantia, D. Merli, S. Protti and M. Fagnoni, *ACS Catal.*, 2022, **12**, 12469–12476.
62 S. C. Mallojjala, V. O. Nyagilo, S. A. Corio and J. S. Hirschi, *J. Am. Chem. Soc.*, 2022, **144**, 17692–17699.
63 S. Morand, W. Lecroq, P. Jubault, S. Lakhdar, J. P. Bouillon and S. C. Bonnaire, *Org. Lett.*, 2022, **24**, 8343–8347.
64 C. Kim, J. Jeong, M. Vellakkaran and S. Hong, *ACS Catal.*, 2022, **12**, 13225–13233.
65 M. Caldarelli, L. Laze, L. Piazza, G. Caputo, M. D. Amici and G. Papeo, *Tetrahedron Lett.*, 2022, **103**, 153978.
66 I. A. MacKenzie, L. Wang, N. P. R. Onuska, O. F. Williams, K. Begam, A. M. Moran, B. D. Dunietz and D. A. Nicewicz, *Nature*, 2020, **580**, 76–80.
67 N. J. Venditto, Y. S. Liang, R. K. E. Mokadem and D. A. Nicewicz, *J. Am. Chem. Soc.*, 2022, **144**, 11888–11896.
68 V. A. Pistritto, M. E. S. Horton and D. A. Nicewicz, *J. Am. Chem. Soc.*, 2020, **142**, 17187–17194.
69 V. A. Pistritto, S. Liu and D. A. Nicewicz, *J. Am. Chem. Soc.*, 2022, **144**, 15118–15131.
70 N. E. S. Tay, W. Chen, A. Levens, V. A. Pistritto, Z. Huang, Z. Wu, Z. Li and D. A. Nicewicz, *Nat. Catal.*, 2020, **3**, 734–742.